


RESEARCH ARTICLE | APRIL 19 2024

Stochastic modeling of blob-like plasma filaments in the scrape-off layer: Correlated amplitudes and velocities

J. M. Losada ; O. Paikina ; O. E. Garcia 



Phys. Plasmas 31, 042514 (2024)

<https://doi.org/10.1063/5.0196938>



APL Quantum
Latest Articles Now Online
Read Now



Stochastic modeling of blob-like plasma filaments in the scrape-off layer: Correlated amplitudes and velocities

Cite as: Phys. Plasmas **31**, 042514 (2024); doi: 10.1063/5.0196938

Submitted: 10 January 2024 · Accepted: 20 March 2024 ·

Published Online: 19 April 2024



View Online



Export Citation



CrossMark

J. M. Losada,^{a)}  O. Paikina,^{b)}  and O. E. Garcia^{c)} 

AFFILIATIONS

Department of Physics and Technology, UiT The Arctic University of Norway, N-9037 Tromsø, Norway

^{a)} Author to whom correspondence should be addressed: juan.m.losada@uit.no

^{b)} Electronic mail: olga.paikina@uit.no

^{c)} Electronic mail: odd.erik.garcia@uit.no

ABSTRACT

A stochastic model for a superposition of uncorrelated pulses with a random distribution of amplitudes, sizes, and velocities is analyzed. The pulses are assumed to move radially with fixed shape and amplitudes decreasing exponentially in time due to linear damping. The pulse velocities are taken to be time-independent but randomly distributed. The implications of a broad distribution of pulse amplitudes and velocities, as well as correlations between these, are investigated. Fast and large-amplitude pulses lead to flattened average radial profiles with order unity relative fluctuations in the scrape-off layer. For theoretically predicted blob velocity scaling relations, the stochastic model reveals average radial profiles similar to the case of a degenerate distribution of pulse velocities but with more intermittent fluctuations. The profile e-folding length is given by the product of the average pulse velocity and the linear damping time due to losses along magnetic field lines. The model describes numerous common features from experimental measurements and underlines the role of large-amplitude fluctuations for plasma-wall interactions in magnetically confined fusion plasmas.

© 2024 Author(s). All article content, except where otherwise noted, is licensed under a Creative Commons Attribution (CC BY) license (<https://creativecommons.org/licenses/by/4.0/>). <https://doi.org/10.1063/5.0196938>

I. INTRODUCTION

One of the main challenges to overcome to achieve economically efficient fusion energy by magnetic confinement is to control plasma and heat transport in the scrape-off layer (SOL) and plasma interactions with material surfaces.^{1–4} A common approach to describe the cross field transport is based on mixing length estimates, assuming scale separation, small relative fluctuations and that the fluxes are proportional to local profile gradients.^{5–11} On this basis, effective diffusivities, or a combination of effective diffusion and radial convection, have been used to characterize the cross field transport in the SOL.^{9–14} Such an approach has been shown to be ill-founded by analysis of both experimental measurement data and first-principles-based turbulence simulations.^{15–20} Indeed, turbulence studies indicate that the cross field transport is dominated by the radial motion of field-aligned plasma filaments.^{21–26} It has since become clear that the cross field transport of particles and heat in the SOL depends on the amplitudes, sizes, velocities, and frequency of occurrence of such blob-like structures as well as correlations between these quantities. Therefore, a

statistical approach is required to describe the resulting fluctuations and transport.^{27–40}

Theoretical investigations of isolated blob-like structures in the scrape-off layer have revealed the physical mechanism for their radial motion and the scaling of their velocity with amplitude, size, and plasma parameters.^{41–60} Scaling theory, as well as numerical simulations of seeded filament structures, have revealed that the radial blob velocity increases with the amplitude. In the so-called inertial regime, there is a linear dependence, while in the sheath-dissipative regime the velocity scales as the square root of the amplitude. In both regimes, there is a saturation of the amplitude dependence when the filament amplitude is much higher than the background level. Such a positive correlation between filament amplitudes and velocities has also been identified in experimental measurement data.⁶¹

The fluctuating plasma parameters in the SOL can be described as a superposition of uncorrelated pulses. Such a statistical description, referred to as a filtered Poisson process, predicts the fluctuations to follow a Gamma distribution with the shape parameter given by the

degree of pulse overlap, that is, the ratio of the average pulse duration and waiting times. This model has been found to be an excellent description of single-point measurements of intermittent fluctuations at the boundary of magnetically confined plasmas. Detailed analysis of experimental measurement data has demonstrated that these pulses have an exponential shape and that the pulse amplitudes are exponentially distributed.^{61–73} This will accordingly be used as assumptions for the stochastic modeling presented in this work.

Recently, the filtered Poisson process was extended to describe the radial motion of blob-like plasma filaments and the resulting radial plasma profiles.^{35–40} Analytical expressions have been derived for the cumulants and the lowest-order statistical moments of the process, elucidating how these depend on the distribution of pulse velocities and their correlations with the amplitudes.⁴⁰ When all pulses have the same velocity, the average radial profile decreases exponentially with radius with an e-folding length given by the product of the radial velocity and the parallel loss time. In Ref. 40, closed-form expressions for the cumulants were obtained for the case of a discrete uniform distribution of pulse velocities independent of the amplitude distribution. In the present contribution, these results are extended to broad and continuous velocity distributions, and correlations between pulse velocities and amplitudes are investigated. Closed analytical expressions are, in general, not available, so the cumulants and the lowest-order moments are calculated numerically.

It is here demonstrated that fast and large-amplitude pulses may lead to nearly flat average radial profiles with order unity relative fluctuations in the scrape-off layer. For theoretically predicted blob velocity scaling relations, the stochastic model reveals average radial profiles similar to the case of a degenerate distribution of pulse velocities but with more frequent large-amplitude fluctuations. This holds for the velocity scaling relations in both the inertial and sheath-dissipative regimes. The average profile e-folding length is given by the product of the average pulse velocity and the linear damping time due to losses along magnetic field lines, while the relative fluctuation level and the skewness and flatness moments increase radially outward. The predictions compare favorably with experimental measurements and underline the role of large-amplitude fluctuations for plasma-wall interactions in magnetically confined fusion plasmas.

This paper is organized as follows. In Sec. II, the theoretical velocity scaling for isolated blob-like filament structures is briefly reviewed, with particular emphasis on the predicted correlations between pulse amplitudes and velocities. The stochastic model describing a superposition of pulses is presented and discussed in Sec. III. In Sec. IV, we present the profiles obtained for various discrete and continuous velocity distributions. For all cases presented in this section, the pulse amplitudes are taken to be exponentially distributed and independent of the velocities. In Sec. V, a correlation between pulse amplitudes and velocities is investigated using a truncated exponential distribution of pulse amplitudes. A discussion of the results and the main conclusions are given in Sec. VI. The change of the pulse amplitude distribution with radial position is discussed in Appendix A. Finally, the role of a distribution of pulse sizes is discussed in Appendix B.

II. BLOB VELOCITY SCALINGS

The stochastic modeling to be presented in Sec. III includes correlations between the amplitude, size, and velocity of blob-like plasma filaments. This is provided by basic mathematical descriptions of filament structures in magnetized plasmas, which are reviewed here.

Their evolution is determined by the plasma vorticity equation, which for a non-uniformly magnetized plasma is given by^{23,74}

$$\mathbf{b} \cdot \nabla \times \left(\rho \frac{d\mathbf{V}}{dt} \right) = \mathbf{B}\mathbf{B} \cdot \nabla \left(\frac{J_{\parallel}}{B} \right) + 2\mathbf{b} \cdot \boldsymbol{\kappa} \times \nabla P, \quad (1)$$

where ρ is the mass density, \mathbf{V} is the fluid velocity, $\mathbf{b} = \mathbf{B}/B$ is the unit vector along the magnetic field \mathbf{B} , J_{\parallel} is the \mathbf{B} -parallel electric current density, $\boldsymbol{\kappa} = (\mathbf{b} \cdot \nabla)\mathbf{b}$ is the magnetic curvature vector, and P is the plasma pressure. In the absence of parallel currents, an order of magnitude estimate with $\nabla_{\perp} \sim 1/\ell$, $d/dt \sim V/\ell$, $\kappa \sim 1/R$, where R is the magnetic field radius of curvature, and $\nabla P/\rho \sim C_s^2 \Delta n/\ell(N + \Delta n)$ immediately gives the inertial velocity scaling^{41–54}

$$\frac{V}{C_s} \sim \left(\frac{2\ell}{R} \frac{\Delta n}{N + \Delta n} \right)^{1/2}, \quad (2)$$

where C_s is the sound speed, ℓ is the cross field blob size, and Δn is the blob amplitude above the background particle density N . In this regime, the velocity increases with the square root of the cross field size. For small relative amplitudes, $\Delta n/N \ll 1$, the velocity has a square root dependence on the amplitude, $V \sim (\Delta n/N)^{1/2}$, while for large relative amplitudes, $\Delta n/N \gg 1$, there is a saturation and the velocity becomes independent of the amplitude.

At the divertor targets, the boundary condition for the parallel electric current density is $J_{\parallel} = enC_s[1 - \exp(e\phi/T_e)]$, where ϕ is the plasma electric potential relative to the sheath and n is the particle density. With $V \sim \phi/Bl$, balancing the parallel current and interchange terms on the right-hand side of Eq. (1) gives the sheath-dissipative velocity scaling^{50–60}

$$\frac{V}{C_s} \sim \frac{2L_{\parallel}\rho_s^2}{R\ell^2} \frac{\Delta n}{N + \Delta n}, \quad (3)$$

where ρ_s is the sound gyroradius and the exponential function in the sheath dissipation term has been linearized. This scaling holds for field-aligned filaments that are electrically connected to the target sheaths. In this regime, the velocity is inversely proportional to the blob size and scales linearly with the relative amplitude for small amplitudes.

More generally, in the intermediate regime between the inertial and sheath-dissipative scalings, an order of magnitude estimate gives a quadratic equation for the blob velocity⁵¹

$$\frac{V^2}{\ell^2} - \frac{2C_s^2}{\ell R} \frac{\Delta n}{N + \Delta n} + \frac{\ell C_s V}{L_{\parallel}\rho_s^2} = 0, \quad (4)$$

where scaling prefactors of order unity has been neglected. The positive root of Eq. (4) is given by

$$\frac{V}{V_*} = \frac{1}{2} \left(\frac{\ell}{\ell_*} \right)^3 \left[-1 + \left(1 + \frac{4\ell_*^5}{\ell^5} \frac{\Delta n}{N + \Delta n} \right)^{1/2} \right], \quad (5)$$

where we have defined a characteristic blob size $\ell_*/\rho_s = (2L_{\parallel}^2/R\rho_s)^{1/5}$ and a corresponding characteristic blob velocity $V_*/C_s = (8\rho_s^2 L_{\parallel}/R^3)^{1/5}$. In Ref. 51, Eq. (5) was found to be an excellent parameterization of the maximum velocity in numerical simulations of isolated blob structures. For large blob sizes, $\ell/\ell_* \gg 1$, the inertial scaling from Eq. (2) is recovered,

$$\frac{V}{V_*} \sim \left(\frac{\ell}{\ell_*} \frac{\Delta n}{N + \Delta n} \right)^{1/2}. \quad (6)$$

Due to the absence of sheath currents, which leads to the dissipation of large-length scales, the velocity increases with the blob size ℓ . For small blob sizes, $\ell/\ell_* \ll 1$, the sheath dissipative scaling from Eq. (3) is given as follows:

$$\frac{V}{V_*} \sim \left(\frac{\ell_*}{\ell} \right)^2 \frac{\Delta n}{N + \Delta n}. \quad (7)$$

The dominating sheath currents lead to strong dissipation of large-length scales, resulting in a velocity that decreases with increasing size. These blob velocity scaling regimes appear to accurately describe experimental measurements in magnetized plasmas, based on both electric probe measurements and gas puff imaging diagnostics as well as numerical simulations of SOL filaments and turbulence.^{75–82} In Sec. V, these theoretically predicted correlations between blob amplitudes and velocities will be used for the stochastic modeling.

III. STOCHASTIC MODEL

Consider a stochastic process with a random variable Φ_K given by a superposition of K uncorrelated pulses,

$$\Phi_K(x, t) = \sum_{k=1}^{K(T)} \phi_k(x, t - s_{0k}), \quad (8)$$

where each pulse ϕ has an arrival time s_0 at the reference position $x = 0$ and satisfies the evolution equation

$$\frac{\partial \phi}{\partial t} + v \frac{\partial \phi}{\partial x} + \frac{\phi}{\tau_{\parallel}} = 0. \quad (9)$$

Here and in the following, we suppress the notation of the k -index except when summation over pulses is explicit. In Eq. (9), v is the pulse velocity and τ_{\parallel} is a constant linear damping time describing drainage due to particle motion along magnetic field lines in the scrape-off layer. All pulses are assumed to have the same shape with the initial condition given by

$$\phi(x, 0) = a_0 \varphi\left(\frac{x}{\ell}\right), \quad (10)$$

where ℓ is the pulse size and a_0 is the pulse amplitude at the reference position $x = 0$. The general solution of Eq. (9) can be written as

$$\phi(x, t) = A(t) \varphi\left(\frac{x - vt}{\ell}\right), \quad (11)$$

where the pulse amplitude decreases exponentially in time due to the linear damping

$$A(t) = a_0 \exp\left(-\frac{t}{\tau_{\parallel}}\right). \quad (12)$$

The stochastic process can accordingly be written as

$$\Phi_K(x, t) = \sum_{k=1}^{K(T)} a_{0k} \exp\left(-\frac{t - s_{0k}}{\tau_{\parallel}}\right) \varphi\left(\frac{x - v_k(t - s_{0k})}{\ell_k}\right). \quad (13)$$

The random variables in this model are as follows:

K : The total number of pulses at the reference position $x = 0$ during a time interval of duration T , taken to be Poisson distributed with average waiting time τ_w ,

$$P_K(K; T) = \frac{1}{K!} \left(\frac{T}{\tau_w}\right)^K \exp\left(-\frac{T}{\tau_w}\right). \quad (14)$$

s : The pulse arrival time s_0 at the reference position $x = 0$, which is uniformly distributed on the time interval $[-T/2, T/2]$ and, thus, given by

$$P_{s_0}(s_0) = \frac{1}{T}. \quad (15)$$

a_0 : The pulse amplitude at the reference position $x = 0$, with marginal probability density function $P_{a_0}(a_0)$.

v : The pulse velocity, is assumed to be positive definite and time-independent with marginal probability density function $P_v(v)$.

ℓ : The pulse size, taken to be the same for all pulses unless otherwise stated (specifically in Appendix B).

A distribution of pulse sizes does not influence the radial variation of the cumulants as long as they are not correlated with the pulse amplitudes or velocities.⁴⁰

In the following, we will consider a one-sided exponential pulse function

$$\varphi(\theta) = \Theta(-\theta) \exp(\theta), \quad (16)$$

where Θ denotes the unit step function,

$$\Theta(\theta) = \begin{cases} 1, & \theta \geq 0, \\ 0, & \theta < 0. \end{cases} \quad (17)$$

The solution of Eq. (9) for an individual pulse can then be written as

$$\phi(x, t) = a_0 \exp\left(-\frac{t}{\tau_{\parallel}}\right) \exp\left(\frac{x - vt}{\ell}\right) \Theta\left(-\frac{x - vt}{\ell}\right), \quad (18)$$

describing the radial motion of a blob-like structure with a steep front and a trailing wake.

A pulse ϕ will arrive at position ζ at time $s_{\zeta} = s_0 + \zeta/v$. The superposition of pulses at this position for a general pulse function $\varphi(\theta)$ can, thus, be written as

$$\Phi_K(\zeta, t) = \sum_{k=1}^{K(T)} a_{\zeta k} \exp\left(-\frac{t - s_{\zeta k}}{\tau_{\parallel}}\right) \varphi\left(-\frac{v_k(t - s_{\zeta k})}{\ell_k}\right), \quad (19)$$

where the pulse amplitudes are given by

$$a_{\zeta} = a_0 \exp\left(-\frac{\zeta}{v\tau_{\parallel}}\right). \quad (20)$$

When all pulses have the same velocity, the amplitudes will have the same probability density function at all radial positions ζ but with a mean value that decreases exponentially with radius. When there is a distribution of pulse velocities, the amplitude distribution will be modified. This is discussed further in Appendix A.

For the one-sided exponential pulse function defined by Eq. (16), the process takes a particularly simple form,

$$\Phi_K(\zeta, t) = \sum_{k=1}^{\kappa(T)} a_{\bar{k}k} \varphi\left(\frac{t - s_{\bar{k}k}}{\tau_k}\right), \quad (21)$$

where the pulse duration τ is given by the harmonic mean of the linear damping and radial transit times,

$$\tau = \frac{\tau_{\parallel} \ell}{v\tau_{\parallel} + \ell}. \quad (22)$$

The average pulse duration $\tau_d = \langle \tau \rangle$ is obtained by averaging over the distribution of pulse sizes and velocities. Equation (19) demonstrates that the process can be regarded as a superposition of pulses with amplitudes that decrease radially outward due to linear damping.

The lowest-order statistical moments of the process can be derived from the cumulants, which are the coefficients in the expansion of the logarithm of the characteristic function. In the case of time-independent velocities and an exponential pulse function, the cumulants of the process Φ_K become⁴⁰

$$\kappa_n(x) = \frac{1}{n\tau_w} \left\langle a_0^n \tau \exp\left(-\frac{nx}{v\tau_{\parallel}}\right) \right\rangle. \quad (23)$$

The averages in this equation are to be performed over the random variables a_0 , v , and ℓ , which, in general, are described by a joint probability distribution. When closed-form expressions for the cumulants are not available, it is straightforward to perform the integrations in Eq. (23) numerically. However, the presence of slow pulses may lead to issues with the existence of cumulants and moments of the process for negative x . Slow pulses with very long radial transit times will have excessively large upstream amplitudes. This results in divergence of cumulants if the velocity probability distribution does not decrease sufficiently fast for small velocities. For this reason, lower truncated amplitude and velocity distributions will be considered in Secs. IV and V. Further discussions on the existence of cumulants are given in Ref. 40.

From the cumulants, we can derive expressions for the lowest-order moments. Specifically, the mean value is given by the first-order cumulant, $\langle \Phi \rangle = \kappa_1(x)$, which has e -folding length $L_{\Phi}(x) = 1/(\text{d} \ln \langle \Phi \rangle / \text{d}x)$. The variance is given by the second-order cumulant, $\Phi_{\text{rms}}^2 = \langle (\Phi - \langle \Phi \rangle)^2 \rangle = \kappa_2(x)$. We further define the skewness and flatness moments, respectively, by

$$S_{\Phi}(x) = \frac{\kappa_3(x)}{\kappa_2^{3/2}(x)}, \quad F_{\Phi}(x) = \frac{\kappa_4(x)}{\kappa_2^2(x)}. \quad (24)$$

For a normally distributed random variable, these two moments vanish. In Secs. IV and V, we will use the relative fluctuation level $\Phi_{\text{rms}}/\langle \Phi \rangle$ and the skewness and flatness moments to quantify the presence of large-amplitude fluctuations in the process.

A variation in the pulse velocities also implies a distribution of pulse durations as described by Eq. (22). When all pulses have the same size, the pulse duration distribution is related to the velocity distribution by the standard rules for the transformation of random variables,

$$P_{\tau}(\tau) = \frac{\ell}{\tau^2} P_v\left(\frac{\ell}{\tau} - \frac{\ell}{\tau_{\parallel}}\right). \quad (25)$$

Since the pulse duration is inversely proportional to the velocity, the average duration is dominated by the small velocities in the case of a random velocity distribution.

When there is a distribution of pulse velocities, the amplitudes and durations will be correlated downstream even if they are independent at the reference position. This is due to their opposite dependence on pulse velocity, given by Eqs. (20) and (22). Fast pulses have short radial transit times and less amplitude reduction due to linear damping. Therefore, a_{ξ} increases with increasing velocity, while τ decreases with increasing velocity. In order to quantify this, we define an effective pulse duration, which is weighted by the pulse amplitude and, therefore, varies with radial position, $\langle a_{\xi} \tau \rangle / \langle a_{\xi} \rangle$. Here, the average is to be taken over the distribution of pulse amplitudes, sizes, and velocities. Similarly, we can define the normalized effective duration by dividing by the average duration, $\langle a_{\xi} \tau \rangle / \langle a_{\xi} \rangle \tau_d$. This is also a measure of the linear correlation between the pulse amplitude and duration.

In Secs. IV and V, it will be demonstrated how a distribution of pulse amplitudes and velocities, and correlations between these, influence the lowest-order moments of the process. It should be noted that the cumulants can be written as $\kappa_n = \langle a_{\xi}^n \tau \rangle / n\tau_w$. Thus, the correlation between pulse amplitudes and durations determines the radial variation of the cumulants and, therefore, also the moments of the process.

IV. INDEPENDENT AMPLITUDES AND VELOCITIES

In this section, we will investigate the case where pulse velocities and amplitudes at the reference position are independent but both have a random distribution. The pulse amplitudes a_0 are assumed to have an exponential distribution, which for $a_0 > 0$ is given by

$$\langle a_0 \rangle P_{a_0}(a_0) = \exp\left(-\frac{a_0}{\langle a_0 \rangle}\right), \quad (26)$$

where $\langle a_0 \rangle$ is the average pulse amplitude. For this distribution, the raw amplitude moments are given by $\langle a_0^n \rangle = n! \langle a_0 \rangle^n$. In the following, various pulse velocity distributions will be considered. Pulse sizes are assumed to have a degenerate distribution, so all pulses have the same size ℓ .

A. Degenerate distribution

In the case of a degenerate distribution, $P_v(v) = \delta(v - \langle v \rangle)$, all pulses have the same velocity $\langle v \rangle$. The cumulants given by Eq. (23) then simplify to

$$\kappa_n(x) = \gamma_* (n-1)! \langle a_0 \rangle^n \exp\left(-\frac{nx}{\langle v \rangle \tau_{\parallel}}\right), \quad (27)$$

where we have defined the intermittency parameter

$$\gamma_* = \frac{\tau_w}{\tau_{\parallel}}, \quad (28)$$

with the pulse duration

$$\tau_w = \frac{\tau_{\parallel} \ell}{\langle v \rangle \tau_{\parallel} + \ell}. \quad (29)$$

The cumulants given by Eq. (27) describe a Gamma distribution with shape parameter γ_* and scale parameter given by the radial pulse amplitude profile

$$\langle a \rangle = \langle a_0 \rangle \exp\left(-\frac{x}{\langle v \rangle \tau_{\parallel}}\right). \quad (30)$$

The probability density function for positive Φ is the Gamma distribution

$$\langle a \rangle P_{\Phi}(\Phi; x) = \frac{1}{\Gamma(\gamma_*)} \left(\frac{\Phi}{\langle a \rangle} \right)^{\gamma_*-1} \exp\left(-\frac{\Phi}{\langle a \rangle}\right), \quad (31)$$

where Γ denotes the Gamma function. The average radial profile is then given by³⁵

$$\langle \Phi \rangle(x) = \gamma_* \langle a_0 \rangle \exp\left(-\frac{x}{\langle v \rangle \tau_{\parallel}}\right), \quad (32)$$

which has e-folding length $L_{\Phi} = \langle v \rangle \tau_{\parallel}$. Moreover, the prefactor for the profile at the reference position is $\langle \Phi \rangle(0) = \gamma_* \langle a_0 \rangle$. The lowest-order normalized moments are in this case radially constant,

$$\frac{\Phi_{\text{rms}}}{\langle \Phi \rangle} = \frac{1}{\gamma_*^{1/2}}, \quad S_{\Phi} = \frac{2}{\gamma_*^{1/2}}, \quad F_{\Phi} = \frac{6}{\gamma_*}. \quad (33)$$

The mean value $\langle \Phi \rangle$ decreases exponentially with radius with an e-folding length given by the product of the radial pulse velocity $\langle v \rangle$ and the linear damping time τ_{\parallel} . The prefactor $\gamma_* \langle a_0 \rangle$ is given by the product of the average pulse amplitude at the reference position and the ratio of the pulse duration and average waiting time. A higher degree of pulse overlap, or larger γ_* , increases the mean value of the process and decreases the relative fluctuation level and intermittency of the process. This defines the reference case in order to compare with a broad distribution of pulse velocities.

B. Discrete uniform distribution

The simplest non-degenerate case to consider is a discrete uniform distribution of pulse velocities, for which they can take two possible values with equal probability,⁴⁰

$$P_v(v; w) = \frac{1}{2} [\delta(v - v_{\min}) + \delta(v - v_{\max})], \quad (34)$$

where $v_{\min} = (1 - w)\langle v \rangle$, $v_{\max} = (1 + w)\langle v \rangle$, $\langle v \rangle$ is the average pulse velocity and w is the width parameter for the distribution with values in the range $0 < w < 1$. The limit $w \rightarrow 0$ corresponds to the case of a degenerate distribution of pulse velocities discussed above. The statistical properties of the process for the discrete uniform distribution were analyzed in detail in Ref. 40 and are summarized here in order to compare with continuous velocity distributions in Subsections IV C and IV D.

For the velocity distribution given by Eq. (34), the pulse duration also has a discrete uniform distribution,

$$P_{\tau}(\tau) = \frac{1}{2} [\delta(\tau - \tau(v_{\min})) + \delta(\tau - \tau(v_{\max}))], \quad (35)$$

with the velocity dependent pulse duration $\tau(v)$ given by Eq. (22). The average pulse duration is given by integration over the discrete distribution,

$$\tau_d = \frac{1}{2} [\tau(v_{\min}) + \tau(v_{\max})]. \quad (36)$$

The average pulse duration increases with w since this implies pulses with lower velocities and correspondingly longer radial transit times ℓ/v_{\min} .

The probability density function for the pulse amplitudes a at position x with the appropriate normalization is for $a > 0$ given by

$$P_a(a; x) = \frac{1}{2a_{\min}} \exp\left(-\frac{a}{a_{\min}}\right) + \frac{1}{2a_{\max}} \exp\left(-\frac{a}{a_{\max}}\right), \quad (37)$$

where we have defined the radial amplitude profile for the slow and fast pulses, respectively, by

$$a_{\min}(x) = \langle a_0 \rangle \exp\left(-\frac{x}{v_{\min} \tau_{\parallel}}\right), \quad (38)$$

$$a_{\max}(x) = \langle a_0 \rangle \exp\left(-\frac{x}{v_{\max} \tau_{\parallel}}\right). \quad (39)$$

The radial profile of the average amplitude given by Eq. (20) is a sum of two exponential functions,

$$\langle a \rangle(x) = \frac{\langle a_0 \rangle}{2} \left[\exp\left(-\frac{x}{v_{\min} \tau_{\parallel}}\right) + \exp\left(-\frac{x}{v_{\max} \tau_{\parallel}}\right) \right]. \quad (40)$$

More generally, the cumulants for the process are given by

$$\kappa_n(x) = \frac{\langle a_0^n \rangle}{2n\tau_w} \left[\tau(v_{\min}) \exp\left(-\frac{nx}{v_{\min} \tau_{\parallel}}\right) + \tau(v_{\max}) \exp\left(-\frac{nx}{v_{\max} \tau_{\parallel}}\right) \right]. \quad (41)$$

In this case, the process $\Phi_K(x, t)$ can be considered as the sum of two filtered Poisson processes, each Gamma distributed with shape parameters $\tau_{\min}/2\tau_w$ and $\tau_{\max}/2\tau_w$, and scale parameters $a_{\min}(x)$ and $a_{\max}(x)$, corresponding, respectively, to the slow and fast pulses. Accordingly, the probability density function for the summed process is given by the convolution of the Gamma distributions for the two sub-processes. At the reference position, the scale parameters for the two sub-processes are the same and the process is Gamma distributed with shape parameter τ_d/τ_w and scale parameter $\langle a_0 \rangle$. Far downstream, the process is dominated entirely by the fast pulses and the probability density function is a Gamma distribution with shape parameter $\tau(v_{\max})/2\tau_w$ and scale parameter $\langle a_0 \rangle \exp(-x/v_{\max} \tau_{\parallel})$.

The discrete uniform velocity distribution is presented in Fig. 1, which is similar to that presented in Ref. 40, together with the radial profile of the mean value, its e-folding length, the relative fluctuation level, and the skewness and flatness moments for various values of the width parameter w . All of these profiles are normalized by their values at the reference position $x=0$ for the reference case of a degenerate distribution of pulse velocities, discussed in Sec. IV A. The profiles, therefore, show how these moments are modified by a distribution of pulse velocities for fixed γ_* , $\langle a_0 \rangle$, and $\langle v \rangle$. In the case of a wide separation of the pulse velocities, the radial profile of the mean value $\langle \Phi \rangle$ is steep at the reference position $x=0$ and becomes significantly flatter far downstream compared to the reference case. The relative fluctuation level and the skewness and flatness moments saturate at the level determined by the fast pulses only, indicated by the dashed lines in Fig. 1.

C. Continuous uniform distribution

Consider next a continuous uniform distribution of pulse velocities, which is non-zero only for velocities in the range $v_{\min} \leq v \leq v_{\max}$ and then given by

$$\langle v \rangle P_v(v; w) = \frac{1}{2w}, \quad (42)$$

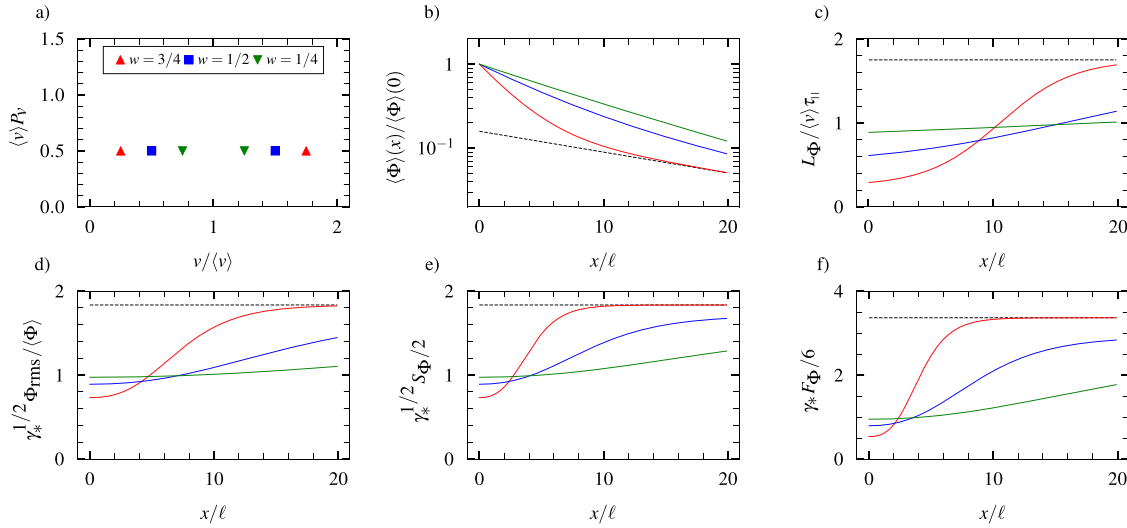


FIG. 1. Results for a discrete uniform distribution of pulse velocities and exponentially distributed pulse amplitudes at $x=0$. Plot panels show (a) velocity distribution, (b) average value, (c) profile scale length, (d) relative fluctuation level, (e) skewness moment, and (f) flatness moment for various values of the width parameter w for the velocity distribution. All radial profiles are normalized with their values at the reference position $x=0$ for the case of a degenerate distribution of pulse velocities. For all radial profiles, the normalized linear damping time is $\langle v \rangle \tau_{||} / \ell = 10$. The dashed lines represent the profiles for the process with only the fast pulses in the case $w = 3/4$.

where $v_{\min} = (1 - w)\langle v \rangle$, $v_{\max} = (1 + w)\langle v \rangle$ and w is the width parameter for the distribution with values in the range $0 < w < 1$. From Eqs. (25) and (42) follows the probability distribution for the pulse duration τ , which is finite in the interval $\tau_{\min} \leq \tau \leq \tau_{\max}$ and given by

$$P_{\tau}(\tau; w) = \frac{\ell}{2w\langle v \rangle \tau^2}, \quad (43)$$

where $\tau_{\min} = \tau_{||} \ell / (v_{\max} \tau_{||} + \ell)$ and $\tau_{\max} = \tau_{||} \ell / (v_{\min} \tau_{||} + \ell)$. The average pulse duration is then given by

$$\tau_d = \frac{\ell}{2w\langle v \rangle} \ln \left(\frac{(1 + w)\langle v \rangle \tau_{||} + \ell}{(1 - w)\langle v \rangle \tau_{||} + \ell} \right). \quad (44)$$

As for the discrete case, the average duration increases with the width parameter w due to the presence of slow pulses with long radial transit times. The power law scaling of the pulse durations in Eq. (43) significantly influences temporal correlations and will result in long-range dependence for a wide distribution.^{30,83}

The continuous uniform velocity distribution as well as the radial profile of the lowest-order moments of the process are presented in Fig. 2. The profiles have the same trend with increasing width parameter w as for the case of a discrete uniform distribution of pulse velocities, but the radial variation is weaker since there is a continuous range of allowed velocities. In particular, the mean value decreases nearly exponentially with radius for large radial positions, close to the case of a degenerate distribution of pulse velocities. However, there is a gradual increase in the relative fluctuation level and, in particular, the skewness and flatness moments with radius. This again demonstrates that the fluctuations become more intermittent for a broad distribution of pulse velocities.

D. Truncated exponential distribution

Finally, we will consider a lower truncated exponential distribution of pulse velocities, which is non-zero for velocities $v \geq v_{\min} = (1 - w)\langle v \rangle$ and then given by

$$\langle v \rangle P_v(v; w) = \frac{1}{w} \exp \left(-\frac{v - (1 - w)\langle v \rangle}{w\langle v \rangle} \right). \quad (45)$$

The truncation parameter w is effectively a width parameter, where the limit $w \rightarrow 0$ corresponds to the case of a degenerate distribution and $w \rightarrow 1$ corresponds to the standard exponential distribution. The truncated exponential distribution is presented in Fig. 3(a) for various values of the width parameter w . The pulse duration distribution is non-zero for $\tau \leq \tau_{\max} = \tau_{||} \ell / (v_{\min} \tau_{||} + \ell)$ and is then given by

$$P_{\tau}(\tau; w) = \frac{\ell}{w\langle v \rangle \tau^2} \exp \left(-\frac{\ell}{w\langle v \rangle \tau} \right) \exp \left(\frac{1 - w}{w} + \frac{\ell}{w\langle v \rangle \tau_{||}} \right). \quad (46)$$

The average pulse duration is

$$\tau_d = \frac{\ell}{w\langle v \rangle} \exp \left(\frac{(1 - w)\langle v \rangle \tau_{||} + \ell}{w\langle v \rangle \tau_{||}} \right) E_1 \left(\frac{(1 - w)\langle v \rangle \tau_{||} + \ell}{w\langle v \rangle \tau_{||}} \right), \quad (47)$$

where E_1 denotes the exponential integral function. This will be discussed further in Sec. IV E.

The radial profiles of the lowest-order moments are presented in Fig. 3 for various values of the width parameter for the truncated exponential velocity distribution. These radial profiles have the same trend as for the case of a continuous uniform distribution of pulse velocities, but the radial variation of the mean value deviates more from exponential for a wide distribution due to the abundance of slow pulses. However, the relative fluctuation level and the skewness and flatness moments are much higher at large radial positions than for a discrete

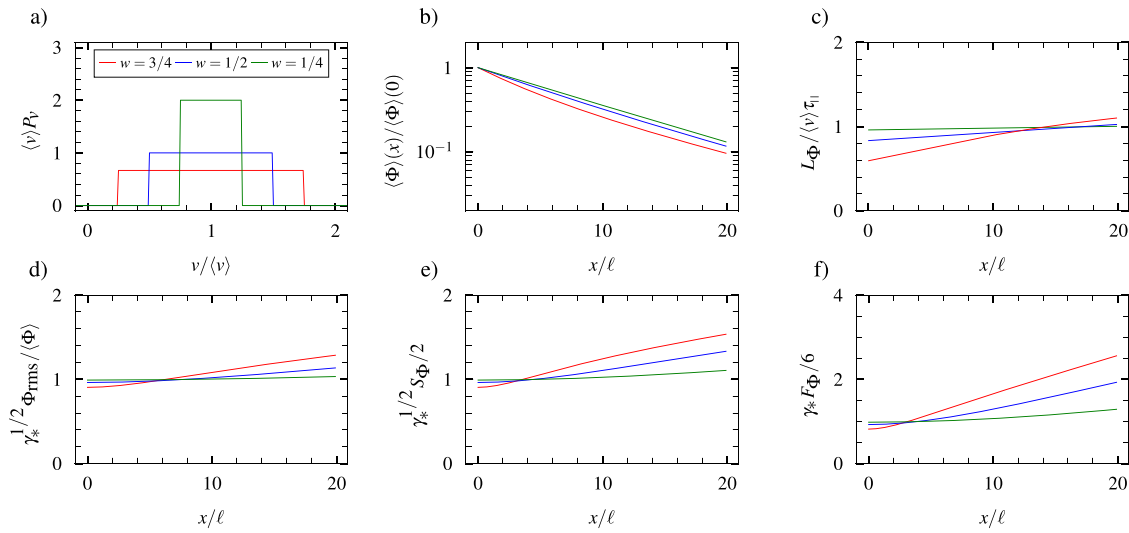


FIG. 2. Results for a continuous uniform distribution of pulse velocities and exponentially distributed pulse amplitudes at $x=0$. Plot panels show (a) velocity distribution, (b) average value, (c) profile scale length, (d) relative fluctuation level, (e) skewness moment, and (f) flatness moment for various values of the width parameter w of the velocity distribution. All radial profiles are normalized with their values at the reference position $x=0$ for the case of a degenerate distribution of pulse velocities. For all radial profiles, the normalized linear damping time is $\langle v \rangle \tau_{||} / \ell = 10$.

uniform velocity distribution, demonstrating strong intermittency of the fluctuations due to fast pulses with short radial transit times.

E. Discussions

As discussed at the end of Sec. III, a distribution of velocities influences both the amplitude and duration of the pulses, described, respectively, by Eqs. (20) and (22). The average duration is dominated by the pulse with small velocities in the case of a wide distribution.

This is demonstrated by the results presented in Fig. 4, which shows the average duration as a function of the width parameter of the velocity distribution when this is discrete uniform, continuous uniform and truncated exponential, corresponding to Eqs. (36), (44), and (47), respectively.

The 1/2 probability for low pulse velocities in the case of a discrete uniform velocity distribution results in a significant increase in the average duration with the width parameter. In the limit $w \rightarrow 1$, this results in nearly stagnant pulses and, in the absence of linear

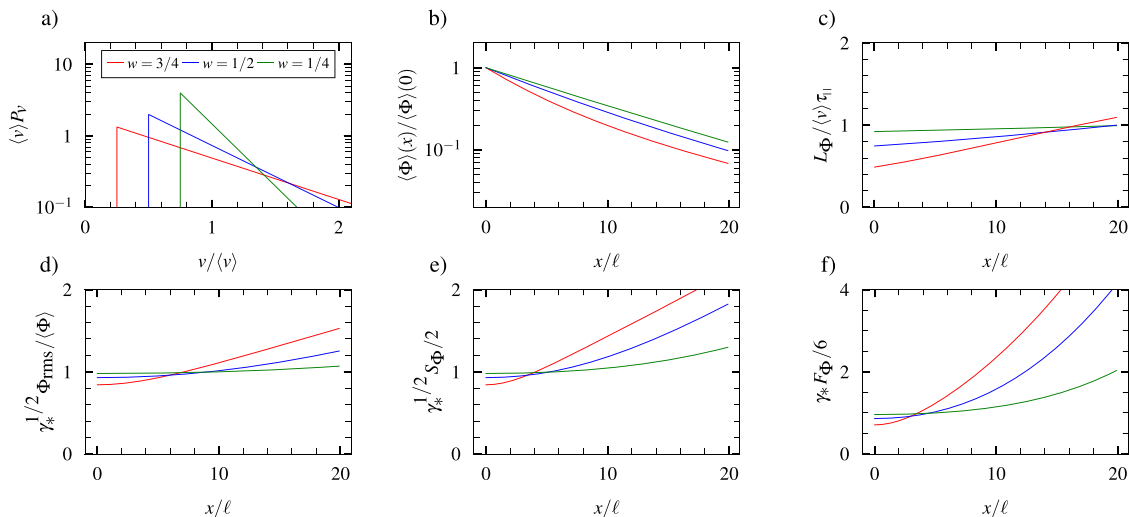


FIG. 3. Results for a lower truncated exponential distribution of pulse velocities and exponentially distributed pulse amplitudes at $x=0$. Plot panels show (a) velocity distribution, and radial profiles of (b) average value, (c) profile scale length, (d) relative fluctuation level, (e) skewness moment, and (f) flatness moment for various values of the width parameter w of the velocity distribution. All radial profiles are normalized with their values at the reference position $x=0$ in the case of a degenerate distribution of pulse velocities. For all radial profiles, the normalized linear damping time is $\langle v \rangle \tau_{||} / \ell = 10$.

06 August 2024 06:17:24

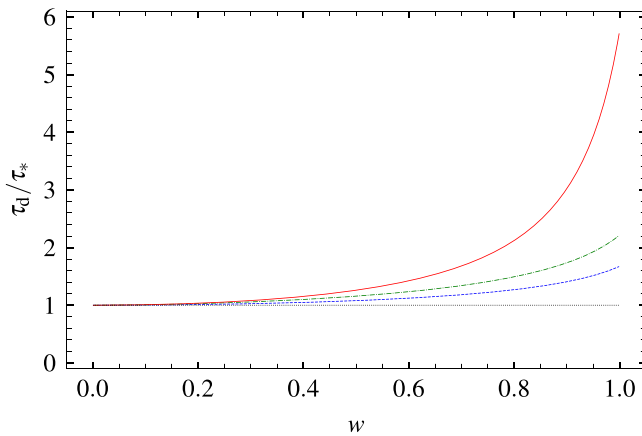


FIG. 4. Average pulse duration as a function of the width parameter w for discrete uniform (red full line), continuous uniform (blue dashed line), and truncated exponential (green dashed-dotted line) distribution of pulse velocities. For all cases, the normalized linear damping time is $\langle v \rangle \tau_{\parallel} / \ell = 10$.

damping, the average pulse duration and, therefore, the mean value of the process diverges.⁴⁰ For the widest continuous velocity distributions, the average pulse duration increases by a factor of approximately two. It is larger for the truncated exponential velocity distribution since this has a higher probability for low pulse velocities, resulting in longer radial transit times.

The increase in the average pulse duration with the width parameter of the velocity distribution also increases the mean value of the process at the reference position, which for uncorrelated pulse amplitudes and durations is given by $\langle \Phi \rangle(0) = (\tau_d / \tau_w) \langle a_0 \rangle$. Note that in the profile figures presented above, this is absorbed in the normalization. However, with increasing average pulse duration, it is also expected that the relative fluctuation level as well as the skewness and flatness moments will be correspondingly reduced at $x=0$, as indeed is seen in Figs. 1–3.

A distribution of pulse velocities further leads to a correlation between pulse amplitudes and durations downstream for the reference position. In Fig. 5, the radial variation of the normalized effective pulse duration is presented for various values of the width parameter of the velocity distribution when this is discrete uniform, continuous uniform, and truncated exponential. At the reference position, the amplitudes and durations are independent, and this is unity. The normalized effective duration decreases radially outward due to the negative correlation between pulse amplitudes and durations. For all cases, the broader the velocity distribution, the stronger the correlation between amplitudes and durations becomes. Accordingly, also the cumulants decrease with an increasing radial coordinate. Far downstream, the process is dominated by the fast pulses, resulting in a short effective duration and radial increase in the relative fluctuation level and the skewness and flatness moments, as shown by the profiles presented above.

V. CORRELATED AMPLITUDES AND VELOCITIES

In this section, we consider the effect of a correlation between pulse velocities and amplitudes at the reference position, in particular, cases where these have a linear or square root relationship and an

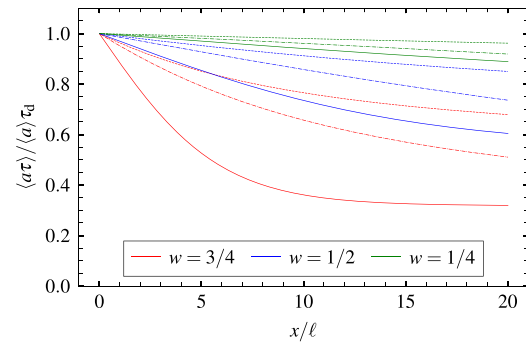


FIG. 5. Radial variation of the linear correlation between pulse amplitudes and durations for various width parameters w for a discrete uniform (full line), continuous uniform (dashed line), and truncated exponential (dashed-dotted line) velocity distribution. For all cases, the amplitude distribution at the reference position $x=0$ is exponential and the normalized linear damping time is $\langle v \rangle \tau_{\parallel} / \ell = 10$.

amplitude saturation, as suggested by the blob velocity scaling estimates presented in Sec. II. Since vanishing pulse velocities are not allowed in the model, we first describe the effect of truncating the exponential amplitude distribution given by Eq. (26).

A. Truncated exponential distribution

Consider again the process with a degenerate velocity distribution, $P_v(v) = \delta(v - \langle v \rangle)$, but a lower truncated exponential distribution of pulse amplitudes, which is nonzero for $a_0 \geq a_{0\min} = (1-w)\langle a_0 \rangle$ and given by

$$\langle a_0 \rangle P_{a_0}(a_0; w) = \frac{1}{w} \exp\left(-\frac{a_0 - (1-w)\langle a_0 \rangle}{w\langle a_0 \rangle}\right). \quad (48)$$

The cumulants for independent pulse amplitudes and velocities can be calculated analytically and are given by

$$\kappa_n(x) = \frac{\gamma}{n} \exp\left(-\frac{nx}{v\tau_{\parallel}}\right) \sum_{i=0}^n \frac{n!}{(n-i)!} [(1-w)\langle a \rangle]^i [w\langle a \rangle]^{n-i}. \quad (49)$$

In the limit $w \rightarrow 1$, this corresponds to a standard exponential amplitude distribution, which is the case described in Sec. IV A. In this limit, the raw amplitude moments are $\langle a_0^n \rangle = n! \langle a_0 \rangle^n$, and the probability density function for the process is a Gamma distribution. In the limit $w \rightarrow 0$, corresponding to a degenerate distribution of pulse amplitudes, the raw amplitude moments are given by $\langle a_0^n \rangle = \langle a_0 \rangle^n$. Accordingly, compared to the reference case with an exponential amplitude distribution, the relative fluctuation level is reduced by a factor $1/\sqrt{2}$, the skewness moment by $\sqrt{2}/3$, and the flatness moment by $1/6$. The variation of these moments with the width parameter is presented in Fig. 6. Each moment is normalized by its value in the case of an exponential distribution of pulse amplitudes.

The mean value $\langle \Phi \rangle$ of the process does not vary with the width parameter w as it only depends on the average amplitude $\langle a_0 \rangle$ and the degree of pulse overlap determined by γ_* . Note that the net effect of decreasing the amplitude width parameter is to decrease intermittency, as is shown by a decrease in all higher-order moments in Fig. 6. This is simply because there is less randomness in the process. In particular,

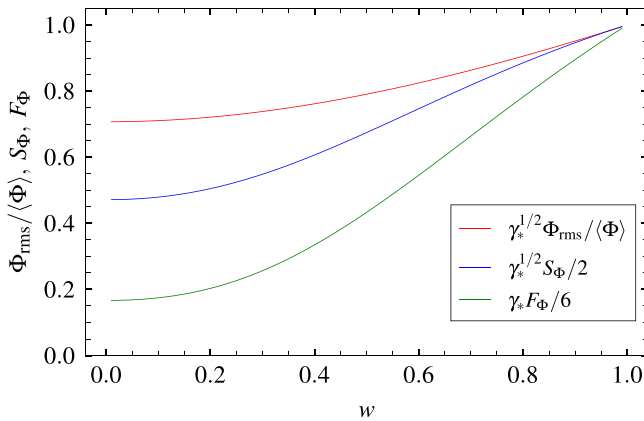


FIG. 6. Relative fluctuation level and skewness and flatness moments of the process for a degenerate distribution of pulse velocities and a lower truncated exponential amplitude distribution with minimum amplitude given by $a_{\min} = (1 - w)\langle a_0 \rangle$ as a function of the width parameter w . Each moment is normalized by the value for a full exponential amplitude distribution.

when all pulses have the same amplitude and velocity, only the pulse arrival times and the number of pulses are randomly distributed.

It is furthermore of interest to consider the case in which pulse amplitudes and velocities are independent at the reference position $x = 0$ but both have a lower truncated exponential distribution with the same width parameter w . This is in contrast to the case in which pulse amplitudes are lower truncated exponentially distributed and the velocities are given by a power law dependence on the pulse amplitudes, which will be analyzed in Subsection V B. The resulting profiles are presented in Fig. 7 for various values of the width parameter. These only differ from those resulting from a lower truncated exponential velocity distribution, shown in Fig. 3, by a constant factor. Thus,

similar to the case discussed in Sec. IV D, the radial increase in the relative fluctuation level and the skewness and flatness moments are much more pronounced for a wide velocity distribution.

B. Power law dependence

As discussed in Sec. II, blob velocity scaling theories demonstrate that the blob velocity depends on the amplitude and size. This motivates the study of cases in which the velocity is given by a power law dependence on the amplitude,

$$\frac{v}{\langle v \rangle} = c_v \left(\frac{a_0}{\langle a_0 \rangle} \right)^\alpha, \quad (50)$$

where the proportionality factor $c_v = \langle a_0 \rangle^\alpha / \langle a_0^\alpha \rangle$ depends on the amplitude distribution. When this is the truncated exponential probability density in Eq. (48), this is given by

$$c_v = \frac{1}{w^\alpha} \frac{\exp(-(1-w)/w)}{\Gamma(1+\alpha, (1-w)/w)}, \quad (51)$$

where Γ here denotes the incomplete Gamma function. In the limit $\alpha \rightarrow 0$, all pulses have the same velocity and this reduces to the case discussed in Subsection IV A. When $\alpha = 1$, the pulse amplitudes and velocities are proportional and both have a truncated exponential distribution.

From the power law relationship in Eq. (50), it follows that the velocity distribution is finite for $v \geq v_{\min} = c_v \langle v \rangle (a_{0\min} / \langle a_0 \rangle)^\alpha$ and then given by

$$\langle v \rangle P_v(v) = \frac{1}{w\alpha c_v} \left(\frac{v}{c_v \langle v \rangle} \right)^{\frac{1-\alpha}{\alpha}} \exp\left(-\frac{1}{w} \left(\frac{v}{c_v \langle v \rangle} \right)^{\frac{1}{\alpha}} - \frac{1-w}{w}\right). \quad (52)$$

In the limit $\alpha \rightarrow 1$, this becomes the truncated exponential distribution given by Eq. (45). From the above velocity distribution, the probability density for the pulse durations follows by use of Eq. (25),

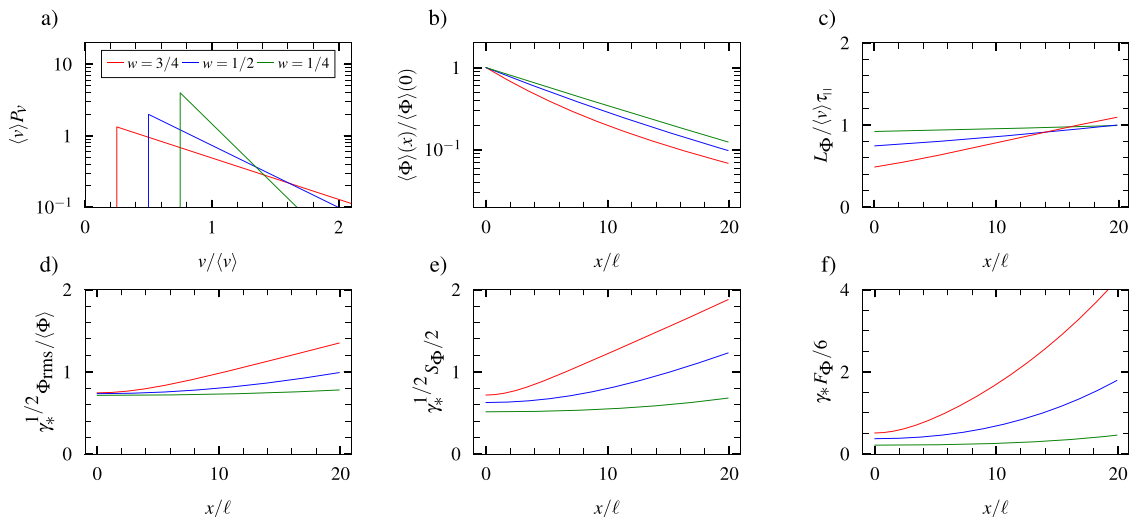


FIG. 7. Results for independent pulse amplitudes and velocities at $x = 0$, both having a lower truncated exponential distribution with the same width parameter w . Plot panels show (a) velocity distribution, and radial profiles of (b) average value, (c) inverse profile scale length, (d) relative fluctuation level, (e) skewness moment, and (f) flatness moment for various values of the width parameter w . All radial profiles are normalized with their values at the reference position $x = 0$ in the case of a degenerate distribution of pulse velocities and an exponential amplitude distribution. For all radial profiles, the normalized linear damping time is $\langle v \rangle \tau_{\parallel} / \ell = 10$.

$$P_\tau(\tau) = \frac{\ell}{w\alpha c_v \langle v \rangle \tau^2} \left(\frac{\ell(\tau_\parallel - \tau)}{c_v \langle v \rangle \tau_\parallel} \right)^{\frac{1-\alpha}{\alpha}} \exp \left(-\frac{1}{w} \left(\frac{\ell(\tau_\parallel - \tau)}{c_v \langle v \rangle \tau_\parallel} \right)^{\frac{1}{\alpha}} - \frac{1-w}{w} \right). \quad (53)$$

For $\alpha = 1$ this gives the same average duration as in Eq. (47), which increases with increasing width parameter for the amplitude distribution. In the limit $\alpha \rightarrow 0$, all pulses have the same velocity and the pulse duration is given by Eq. (29), independent of the width of the amplitude distribution.

The marginal velocity probability density function and the radial profile of the lowest-order moments are presented in Fig. 8 for $\alpha = 1/2$ and $\alpha = 1$, and for various values of the width parameter for a lower truncated exponential distribution. For all cases, the radial variation of the mean $\langle \Phi \rangle$ is nearly exponential with an e-folding length close to $\langle v \rangle \tau_\parallel$, the same as for the reference case with a degenerate velocity distribution. The decrease in the mean value due to a wide velocity distribution as found in Sec. IV is balanced by the strong correlation between pulse amplitudes and sizes. Thus, fast and large-amplitude pulses result in a large mean value as well as a high relative fluctuation level and skewness and flatness moments that increase radially outward.

C. Amplitude saturation

The blob velocity scaling theory suggests a saturation of the velocity dependence on pulse amplitude when these become large compared to any background level, as described by Eq. (5). In order to investigate this, we finally consider the scaling relationship

$$\frac{v}{\langle v \rangle} = c_v \left(\frac{a_0}{\langle a_0 \rangle + a_0} \right)^\alpha, \quad (54)$$

and a truncated exponential distribution for the pulse amplitudes a_0 . The marginal velocity probability density function and the radial profile of the lowest-order moments are presented in Fig. 9 for $\alpha = 1/2$

and $\alpha = 1$, and for various values of the width parameter. Again we observe that for all cases, the radial variation of the mean $\langle \Phi \rangle$ is nearly exponential and similar to the reference case where all pulses have the same velocity. Thus, the e-folding length is determined by the average pulse velocity and has a weak dependence on the width of the distribution. The relative fluctuation level as well as the skewness and flatness moments increase radially outward but not as strongly as for the power law scaling $v \sim a_0^\alpha$ due to the saturation for large pulse amplitudes described by Eq. (54).

D. Discussions

As discussed in Sec. IV E, the pulse amplitudes and durations become correlated downstream from the reference position $x = 0$. With a power law relationship between pulse amplitudes and velocities as discussed above, there is an initial correlation between these at the reference position. This can be calculated analytically for the power law scaling given by Eq. (50), which at the reference position for $\alpha = 1$ gives

$$\langle a_0 \tau \rangle = \frac{\ell \langle a_0 \rangle}{\langle v \rangle} \left(1 - \frac{\tau_d}{\tau_\parallel} \right), \quad (55)$$

where the average pulse duration is given by Eq. (47). In Fig. 10, the radial variation of the normalized effective pulse duration is presented for the power law scaling given by Eq. (50) and various values of the width parameter w . At the reference position, the correlation becomes stronger with increasing width parameter for the amplitude distribution. This should be compared to Fig. 5, which shows the effective duration in the case of uncorrelated pulse amplitudes and velocities at the reference position. In both cases, the normalized effective pulse duration decreases radially outward, being increasingly dominated by large-amplitude, fast pulses.

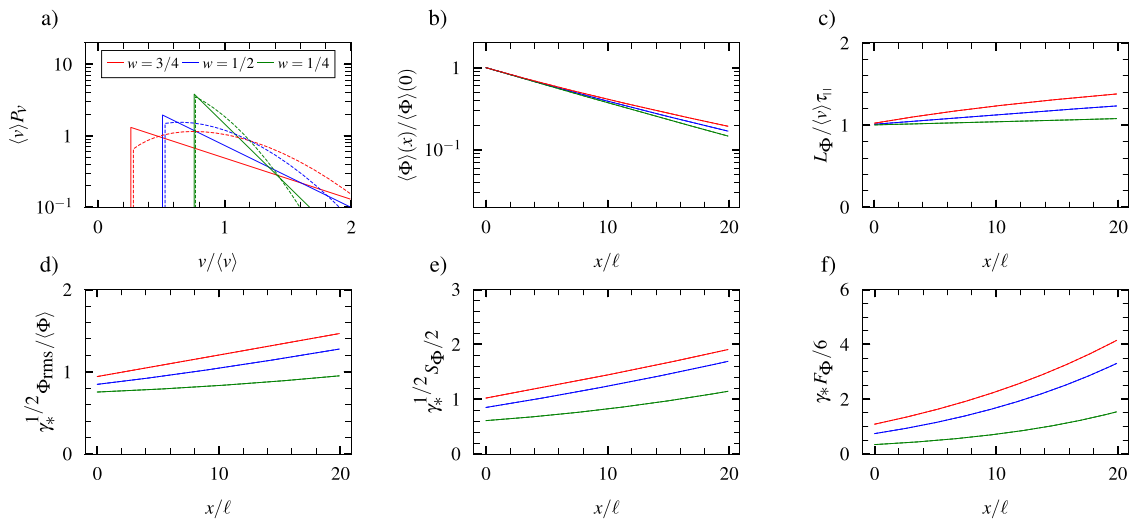


FIG. 8. Results for correlated pulse amplitudes and velocities, $v \sim (a_0/\langle a_0 \rangle)^\alpha$, with $\alpha = 1/2$ (broken lines) and $\alpha = 1$ (full lines), for a lower truncated exponential amplitude distribution with width parameter w at $x = 0$. Plot panels show (a) marginal velocity distribution and radial profiles of (b) average value, (c) profile scale length, (d) relative fluctuation level, (e) skewness moment, and (f) flatness moment for various values of the width parameter w . All radial profiles are normalized with their values at the reference position $x = 0$ in the reference case of a degenerate distribution of pulse velocities and an exponential amplitude distribution. For all radial profiles, the normalized linear damping time is $\langle v \rangle \tau_\parallel / \ell = 10$.

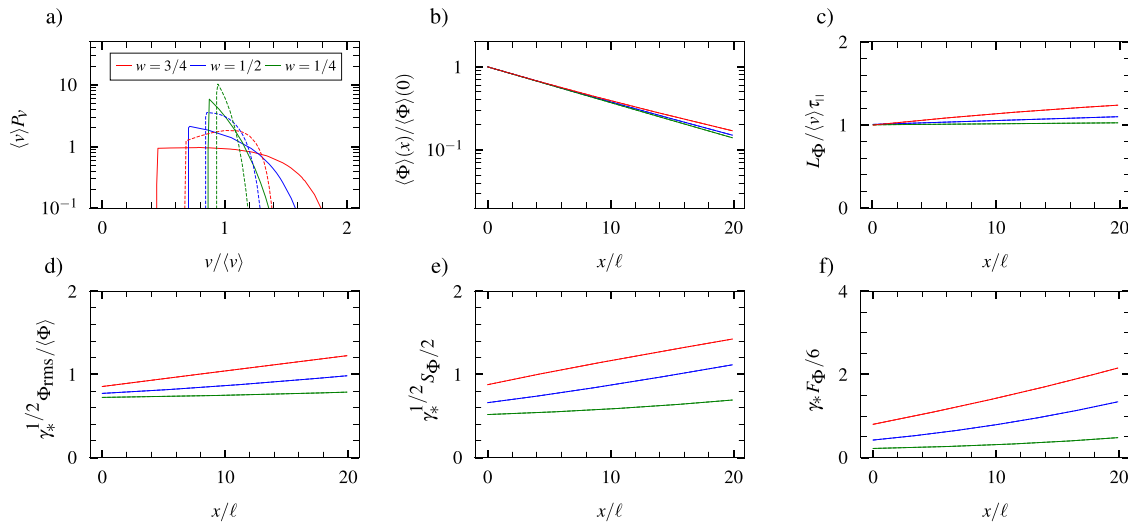


FIG. 9. Results for correlated pulse amplitudes and velocities, $v \sim [a_0/(\langle a_0 \rangle + a_0)]^\alpha$, with $\alpha = 1/2$ (broken lines) and $\alpha = 1$ (full lines), for a lower truncated exponential amplitude distribution with width parameter w at $x = 0$. Plot panels show (a) marginal velocity distribution and radial profiles of (b) average value, (c) profile scale length, (d) relative fluctuation level, (e) skewness moment, and (f) flatness moment for various values of the width parameter w . All radial profiles are normalized with their values at the reference position $x = 0$ in the reference case of a degenerate distribution of pulse velocities and an exponential amplitude distribution. For all radial profiles, the normalized linear damping time is $\langle v \rangle \tau_{\parallel} / \ell = 10$.

In conclusion, there are several mechanisms which modify the cumulants and moments and their variation with radial position. First, a distribution of pulse velocities increases the average pulse duration, which is dominated by slow pulses. Second, since pulse amplitudes and durations have opposite dependence on pulse velocity, a distribution of velocities leads to a negative correlation of these and a radial increase in the relative fluctuation level and the skewness and flatness moments. Third, an initial correlation between amplitudes and velocities further reduces the cumulants and moments. Finally, a distribution of pulse velocities will also change the downstream amplitude distribution. This mechanism is discussed in [Appendix A](#).

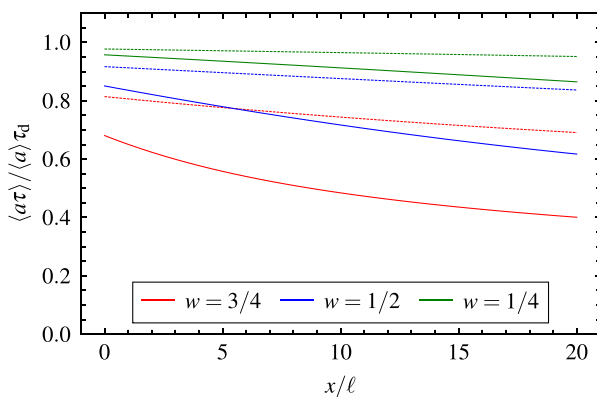


FIG. 10. Radial variation of the linear correlation between pulse amplitudes and durations for the power law scaling $v \sim a^\alpha$ with $\alpha = 1/2$ (broken lines) and $\alpha = 1$ (full lines) for a truncated exponential amplitude distribution with width parameter w . The normalized linear damping time is $\langle v \rangle \tau_{\parallel} / \ell = 10$.

VI. DISCUSSION AND CONCLUSIONS

Experimental measurements at the boundary of magnetically confined plasmas have demonstrated that the particle density profile in the SOL has a shoulder-like structure.^{84–99} In the near SOL, close to the magnetic separatrix, the profile is steep and has moderate fluctuation levels. Further out in the far SOL, the profile has an exponential decay with a much longer scale length and an order unity relative fluctuation level. As the empirical discharge density limit is approached, the break point between the near and the far SOL regions moves radially inward and the far SOL profile becomes flatter. This change in the profile is generally attributed to radial transport caused by blob-like filament structures in the far SOL. Thus, understanding and predicting profile broadening and flattening, and the associated enhanced plasmas–surface interactions, requires a detailed investigation of these fluctuations.

The stochastic modeling presented here shows that an exponential average profile follows from a superposition of uncorrelated pulses which all have the same radial velocity, $\langle \Phi \rangle(x) = \gamma_* \langle a_0 \rangle \exp(-x/\langle v \rangle \tau_{\parallel})$. In this reference case, the profile e-folding length is given by the product of the radial pulse velocity and the linear damping time due to particle motion along magnetic field lines in the SOL. Accordingly, faster blobs and a longer magnetic connection length result in a flatter far SOL profile, in agreement with experimental measurement. Higher core plasma density or longer connection length leads to higher collisionality in the SOL, and the blob velocity scaling regime is expected to transition from sheath dissipative to inertial, resulting in higher radial velocities and thereby a flatter profile. This is believed to be a dominant mechanism for shoulder formation, large relative fluctuations and enhanced plasma wall–interactions at the outboard midplane of toroidal plasmas.

At the reference position, the prefactor for the profile is given by the product of the average pulse amplitude and the ratio of the pulse duration and average waiting time. The process is strongly intermittent

with large relative fluctuations when the latter ratio is small, implying little overlap of pulses. When the amplitudes are exponentially distributed, the process has a Gamma probability density with the mean amplitude as the scale parameter and the ratio of the pulse duration and the average waiting time as the shape parameter. From this, it follows that the relative fluctuation level and the skewness and flatness moments are radially constant. The present understanding of the blob formation process is limited, and there are no first-principles based predictions for the average pulse waiting time or the average amplitude. However, it is anticipated that the blob structures are formed at the transition region from the near to the far SOL; thus, their average amplitude will increase as the far SOL profile broadens and flattens. This again leads to higher velocities, further contributing to profile flattening and broadening.

A random distribution of pulse velocities significantly modifies the stochastic process. It leads to longer average pulse durations, thereby increasing the degree of pulse overlap and the mean value of the process. The relative fluctuation level and the skewness and flatness moments are reduced close to the reference position due to longer pulse durations, as seen in Figs. 1–3 and 7–9. However, there will also be a negative correlation between pulse amplitudes and durations downstream from the reference position. This results in a shorter effective pulse duration and the process becomes dominated by the fast pulses, which have short radial transit times and undergo less linear damping due to parallel transport. As a result, the relative fluctuation level and the skewness and flatness moments increase radially outward. In the simplest case of a discrete uniform velocity distribution, the average profile has a bi-exponential shape, as shown in Fig. 1, resembling the near and far SOL regions typically measured at the boundary of magnetically confined plasmas.

For pulse velocities with a continuous distribution but independent of pulse amplitudes, as discussed in Sec. IV, the average profile is, in general, non-exponential with a shorter e-folding length than the reference case with a degenerate velocity distribution. However, the relative fluctuation level and the skewness and flatness moments are generally higher and increase radially outward. The intermittency of the process is further amplified when there is a correlation between pulse amplitudes and velocities. The blob velocity scaling theory presented in Sec. II suggests that the pulse velocity depends linearly on the amplitude in the inertial regime or as the square root of the amplitude in the sheath dissipative regime. Moreover, there is a saturation of the amplitude dependence for large relative amplitudes. However, in all these cases and for any width parameter of the amplitude distribution, the average radial profile is close to that of the reference case where all pulses have the same velocity, as shown in Sec. V. The high average plasma density, long profile scale length and high relative fluctuation level in the SOL underline the importance of blob-like plasma filaments for profile flattening and plasma contact with limiter structures and the main chamber walls.

The stochastic model presented here provides a unique statistical framework for analyzing and interpreting fluctuation measurements from the boundary region of magnetically confined plasmas.^{27–40} It should be noted that there is no background or equilibrium plasma in the SOL according to the model. The mean value is entirely due to blob-like filament structures moving radially outward. Numerous investigations have demonstrated that both the underlying assumptions of the model as well as its predictions are in excellent agreement with experimental measurements from single-point recordings.^{61–73}

This includes pulses arriving according to a Poisson process with an exponential distribution of pulse waiting times, an exponential pulse function, and an exponential distribution of pulse amplitudes. Similarly, the stochastic model can be used for validation of first principles-based turbulence simulations of the boundary region.¹⁰⁰ There are numerous other applications of the stochastic model for analysis of transport phenomena in the SOL. This includes the treatment of time-dependent pulse velocities, which are proportional to the instantaneous amplitudes, coupling to a two-point model to address the role of large-amplitude fluctuations for parallel transport, extension to two spatial dimensions and optimization of time delay estimates of blob velocities, and adding interactions with neutral particles to investigate the impact of filament structures on ionization and recombination processes in the SOL. This will lead to a deeper understanding of plasma dynamics and transport in the SOL, guiding and improving transport modeling efforts which use effective diffusivities and convection to describe radial profiles and plasma–surface interactions in magnetically confined plasmas.

ACKNOWLEDGMENTS

This work was supported by the UiT Aurora Centre Program, UiT The Arctic University of Norway (2020). The authors acknowledge discussions with A. Theodorsen.

AUTHOR DECLARATIONS

Conflict of Interest

The authors have no conflicts to disclose.

Author Contributions

J. M. Losada: Conceptualization (equal); Data curation (equal); Formal analysis (equal); Investigation (equal); Methodology (equal); Project administration (equal); Resources (equal); Software (equal); Validation (equal); Visualization (equal); Writing – original draft (equal); Writing – review & editing (equal). **O. Paikina:** Validation (equal); Visualization (equal). **O. E. Garcia:** Conceptualization (equal); Formal analysis (equal); Funding acquisition (equal); Investigation (equal); Methodology (equal); Project administration (equal); Resources (equal); Supervision (equal); Validation (equal); Writing – original draft (equal); Writing – review & editing (equal).

DATA AVAILABILITY

Data sharing is not applicable to this article as no new data were created or analyzed in this study.

APPENDIX A: AMPLITUDE DISTRIBUTION

The dominant mechanism for radial variation of the relative fluctuation level and the skewness and flatness moments is the correlation between pulse amplitudes and durations when there is a broad distribution of pulse velocities. However, the change in the amplitude distribution with radial position will also influence the moments of the process.

The pulse amplitude at any position ξ is given by Eq. (20). In the case of a random distribution of pulse velocities v , the

amplitudes a_ξ at position ξ are given by the product of two random variables. The probability density of the product of two independent, non-negative random variables is given by the Mellin convolution of the two corresponding densities. Assuming there is no correlation between amplitudes and velocities, the distribution of a_ξ is, thus, given by

$$P_{a_\xi}(a_\xi) = \int_0^\infty \frac{da_0}{a_0} P_{a_0}(a_0) P_u\left(\frac{a_\xi}{a_0}\right), \quad (\text{A1})$$

where P_u is the probability distribution of the random variable $u = \exp(-\xi/v\tau_{\parallel})$.

As an example, consider an exponential distribution for the pulse amplitudes a_0 given by Eq. (26) and a truncated exponential distribution of pulse velocities. The exponential transform of the scaled reciprocal random variable $-\xi/v\tau_{\parallel}$ results in a new random variable u , which for $\xi > 0$ has the probability density

$$P_u(u) = \frac{\xi}{w\langle v \rangle \tau_{\parallel}} \frac{1}{u \ln^2 u} \exp\left(\frac{(1-w)\langle v \rangle + \xi/\tau_{\parallel} \ln u}{w\langle v \rangle}\right), \quad (\text{A2})$$

for u in the range $u_{\min} \leq u < 1$, where

$$u_{\min} = \exp\left(-\frac{\xi}{\tau_{\parallel}(1-w)\langle v \rangle}\right). \quad (\text{A3})$$

Accordingly, the lower integration limit on a_0 in Eq. (A1) is a_ξ the upper limit is a_ξ/u_{\min} . As the distributions P_{a_0} and P_u are known, we can determine P_{a_ξ} at the radial position ξ .

The amplitude probability distribution function P_{a_ξ} is presented in Fig. 11 for various radial positions ξ for the truncated exponential velocity distribution with width parameter $w = 3/4$. At $\xi = 0$, the distribution is by definition exponential. The downstream amplitude distribution is peaked for small amplitudes since slow pulses have long radial transit times and are strongly depleted by linear damping. Far downstream, the distribution is well described by a Gamma distribution with a shape parameter $\alpha < 1$,

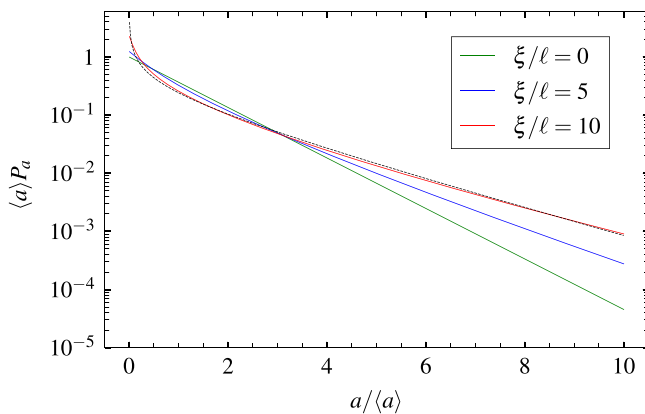


FIG. 11. Probability density function of the pulse amplitudes for a truncated exponential distribution of pulse velocities with width parameter $w = 3/4$ at various radial positions in the case $\langle v \rangle \tau_{\parallel} / \ell = 10$. The dashed line shows a Gamma distribution with shape parameter $\alpha = 1/2$.

$$\langle a_\xi \rangle P_{a_\xi}(a_\xi) = \frac{1}{\Gamma(\alpha)} \left(\frac{a_\xi}{\langle a_\xi \rangle}\right)^{\alpha-1} \exp\left(-\frac{a_\xi}{\langle a_\xi \rangle}\right), \quad (\text{A4})$$

where the average amplitude $\langle a_\xi \rangle$ at the position ξ is the scale parameter of the distribution. For this probability density, the amplitude moments are given by $\langle a_\xi^n \rangle = \langle a_\xi \rangle^n \Gamma(n + \alpha) / \Gamma(\alpha)$.

In order to quantify how the strongly peaked amplitude distribution modifies the process, consider a superposition of uncorrelated, exponential pulses³⁰

$$\Psi_K(t) = \sum_{k=1}^{K(T)} a_{\xi k} \psi\left(\frac{t - s_k}{\tau_d}\right), \quad (\text{A5})$$

with Gamma distributed amplitudes given by Eq. (A4) and an exponential pulse function ψ with fixed duration τ_d . The lowest-order moments for this process are readily calculated as³³

$$\langle \Psi \rangle = \gamma \alpha \langle a_\xi \rangle, \quad (\text{A6a})$$

$$\Psi_{\text{rms}}^2 = \frac{1}{2} \gamma \alpha (1 + \alpha) \langle a_\xi^2 \rangle, \quad (\text{A6b})$$

$$S_\Psi = \frac{2^{3/2}}{3\gamma^{1/2}} \frac{\alpha + 2}{[\alpha(1 + \alpha)]^{1/2}}, \quad (\text{A6c})$$

$$F_\Psi = \frac{1}{\gamma} \frac{(2 + \alpha)(3 + \alpha)}{\alpha(1 + \alpha)}. \quad (\text{A6d})$$

When the shape parameter α is small, the relative fluctuation level and the skewness and flatness moments are very high due to the occasional appearance of large-amplitude pulses. In fact, in the limit $\alpha \rightarrow 0$, the shape parameter has the same influence on these moments as the intermittency parameter γ that determines the degree of pulse overlap. However, as discussed in Sec. III, the main mechanism for the radial increase in relative fluctuation level and the skewness and flatness moments is the correlation between pulse amplitudes and durations. In Ref. 40, this was explicitly demonstrated for a discrete uniform velocity distribution.

APPENDIX B: SIZE DISTRIBUTION

A random distribution of pulse sizes with modify the pulse durations and lead to more randomness in the process. Consider truncated exponentially distributed amplitudes with width parameter $3/4$, continuous uniformly distributed sizes ℓ in the range $\ell_{\min} \leq \ell \leq \ell_{\max}$,

$$\langle \ell \rangle P_\ell(\ell; w) = \frac{1}{2w}, \quad (\text{B1})$$

where $\ell_{\min} = (1 - w)\langle \ell \rangle$ and $\ell_{\max} = (1 + w)\langle \ell \rangle$, and pulse velocities given by Eq. (5),

$$\frac{v}{\langle v \rangle} = \frac{c_v}{2} \frac{\ell^3}{\langle \ell \rangle^3} \left[-1 + \left(1 + \frac{4\langle \ell \rangle^5}{\ell^5} \frac{a_0}{\langle a_0 \rangle + a_0} \right)^{1/2} \right], \quad (\text{B2})$$

where c_v is a normalization constant. The velocity distribution and resulting profiles of the lowest-order moments are presented in Fig. 12. Compared to Fig. 9, the velocity distribution is broader for a wide amplitude distribution. As a result, the e-folding length for the

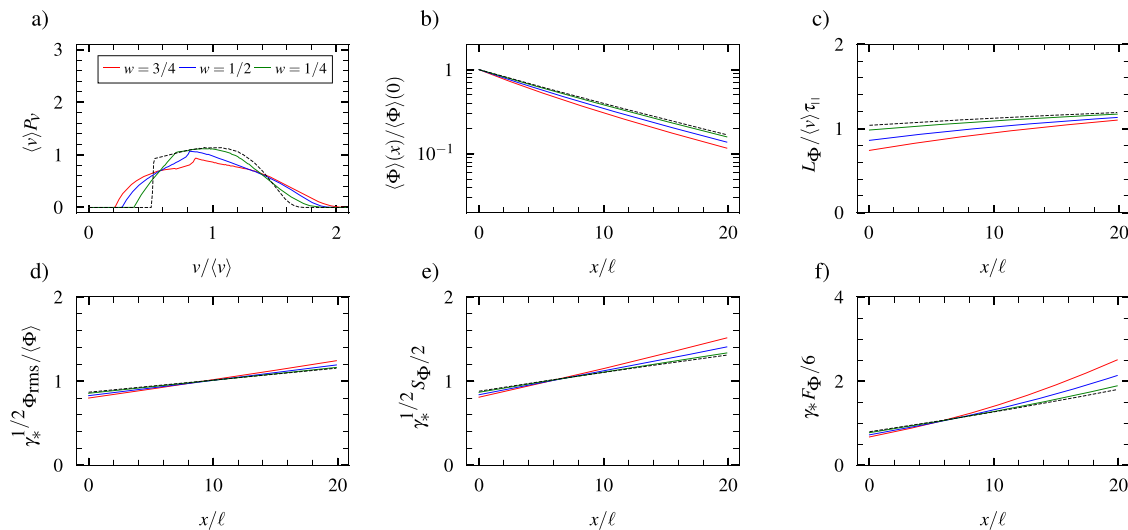


FIG. 12. Results for correlated pulse amplitudes, sizes and velocities given by Eq. (B2) with a truncated exponential amplitude distribution with width parameter 3/4 and a uniform size distribution with width parameter w . Plot panels show (a) marginal velocity distribution and radial profiles of (b) average value, (c) profile scale length, (d) relative fluctuation level, (e) skewness moment, and (f) flatness moment for various values of the width parameter w . All radial profiles are normalized with their values at the reference position $x = 0$ in the case of a degenerate distribution of pulse velocities. The dashed lines show the profiles for a degenerate distribution of pulse sizes. For all radial profiles, the normalized linear damping time is $\langle v \rangle \tau_\parallel / \ell = 10$.

profile is shorter and the mean value lower than for the reference case with a degenerate velocity distribution. However, the high velocity pulses result in larger fluctuation amplitudes and higher skewness and flatness moments for a wide size distribution.

REFERENCES

- ¹P. C. Stangeby, *The Plasma Boundary of Magnetic Fusion Devices* (Institute of Physics Publishing, 2000).
- ²W. Fundamenski, *Power Exhaust in Fusion Plasmas* (Cambridge University Press, 2014).
- ³S. Krasheninnikov, A. Smolyakov, and A. Kukushkin, *On the Edge of Magnetic Fusion Devices* (Springer, 2020).
- ⁴F. Militello, *Boundary Plasma Physics: An Accessible Guide to Transport, Detachment, and Divertor Design* (Springer, 2023).
- ⁵J. W. Connor, "Invariance principles and plasma confinement," *Plasma Phys. Controlled Fusion* **30**, 619–650 (1988).
- ⁶J. W. Connor, G. F. Counsell, S. K. Erements, S. J. Fielding, B. LaBombard, and K. Morel, "Comparison of theoretical models for scrape-off layer widths with data from COMPASS-D, JET and Alcator C-Mod," *Nucl. Fusion* **39**, 169–188 (1999).
- ⁷J. W. Connor and O. P. Pogutse, "On the relationship between mixing length and strong turbulence estimates for transport due to drift turbulence," *Plasma Phys. Controlled Fusion* **43**, 155 (2001).
- ⁸J. Weiland, "Review of mixing length estimates and effects of toroidicity in a fluid model for turbulent transport in tokamaks," *Plasma Phys. Rep.* **42**, 502–513 (2016).
- ⁹P. C. Stangeby, "Tutorial on some basic aspects of divertor physics," *Plasma Phys. Controlled Fusion* **42**, 271–291 (2000).
- ¹⁰P. C. Stangeby, "Modeling plasma contact with the main vessel walls of a divertor tokamak," *Phys. Plasmas* **9**, 3489 (2002).
- ¹¹V. Naulin, "Turbulent transport and the plasma edge," *J. Nucl. Mater.* **363–365**, 24–31 (2007).
- ¹²J. L. Terry, B. LaBombard, B. Lipschultz, M. J. Greenwald, J. E. Rice, and S. J. Zweben, "The scrape-off layer in Alcator C-Mod: Transport, turbulence, and flows," *Fusion Sci. Technol.* **51**, 342–356 (2007).
- ¹³A. Y. Pigarov, S. I. Krasheninnikov, T. D. Rognlien, M. J. Schaffer, and W. P. West, "Tokamak edge plasma simulation including anomalous cross-field convective transport," *Phys. Plasmas* **9**, 1287 (2002).
- ¹⁴M. V. Umansky, P. Popovich, T. A. Carter, B. Friedman, and W. M. Nevins, "Numerical simulation and analysis of plasma turbulence the large plasma device," *Phys. Plasmas* **18**, 055709 (2011).
- ¹⁵B. LaBombard, R. L. Boivin, M. Greenwald, J. Hughes, B. Lipschultz, D. Mossessian, C. S. Pitcher, J. L. Terry, and S. J. Zweben, "Particle transport in the scrape-off layer and its relationship to discharge density limit in Alcator C-Mod," *Phys. Plasmas* **8**, 2107–2117 (2001).
- ¹⁶O. E. Garcia, R. A. Pitts, J. Horacek, A. H. Nielsen, W. Fundamenski, J. P. Graves, V. Naulin, and J. J. Rasmussen, "Turbulent transport in the TCV SOL," *J. Nucl. Mater.* **363–365**, 575–580 (2007).
- ¹⁷O. E. Garcia, J. Horacek, R. A. Pitts, A. H. Nielsen, W. Fundamenski, V. Naulin, and J. J. Rasmussen, "Fluctuations and transport in the TCV scrape-off layer," *Nucl. Fusion* **47**, 667–676 (2007).
- ¹⁸S. I. Krasheninnikov, A. Y. Pigarov, T. K. Soboleva, and D. L. Rudakov, "Strongly intermittent edge plasma transport: Issues with modeling and interpretation of experimental data," *Phys. Plasmas* **16**, 014501 (2009).
- ¹⁹S. J. Zweben, W. M. Davis, S. M. Kaye, J. R. Myra, R. E. Bell, B. P. LeBlanc, R. J. Maqueda, T. Munsat, S. A. Sabbagh, Y. Sechrest, and D. P. Stotler, "Edge and SOL turbulence and blob variations over a large database in NSTX," *Nucl. Fusion* **55**, 093035 (2015).
- ²⁰Y. Marandet, N. Nace, M. Valentinuzzi, P. Tamain, H. Bufferand, G. Ciraolo, P. Genesis, and N. Mellet, "Assessment of the effects of scrape-off layer fluctuations on first wall sputtering with the TOKAM-2D turbulence code," *Plasma Phys. Controlled Fusion* **58**, 114001 (2016).
- ²¹D. A. D'Ippolito, J. R. Myra, S. I. Krasheninnikov, G. Q. Yu, and A. Y. Pigarov, "Blob transport in the tokamak scrape-off-layer," *Contrib. Plasma Phys.* **44**, 205–216 (2004).
- ²²S. J. Zweben, J. A. Boedo, O. Grulke, C. Hidalgo, B. LaBombard, R. J. Maqueda, P. Scarin, and J. L. Terry, "Edge turbulence measurements in toroidal fusion devices," *Plasma Phys. Controlled Fusion* **49**, S1–S23 (2007).
- ²³S. I. Krasheninnikov, D. A. D'Ippolito, and J. R. Myra, "Recent theoretical progress in understanding coherent structures in edge and SOL turbulence," *J. Plasma Phys.* **74**, 679–717 (2008).

- ²⁴O. E. Garcia, "Blob transport in the plasma edge: A review," *Plasma Fusion Res.* **4**, 019 (2009).
- ²⁵J. A. Boedo, "Edge turbulence and SOL transport in tokamaks," *J. Nucl. Mater.* **390–391**, 29–37 (2009).
- ²⁶D. A. D'Ippolito, J. R. Myra, and S. J. Zweben, "Convective transport by intermittent blob-filaments: Comparison of theory and experiment," *Phys. Plasmas* **18**, 060501 (2011).
- ²⁷O. E. Garcia, "Stochastic modeling of intermittent scrape-off layer plasma fluctuations," *Phys. Rev. Lett.* **108**, 265001 (2012).
- ²⁸R. Kube and O. E. Garcia, "Convergence of statistical moments of particle density time series in scrape-off layer plasmas," *Phys. Plasmas* **22**, 012502 (2015).
- ²⁹A. Theodorsen and O. E. Garcia, "Level crossings, excess times, and transient plasma-wall interactions in fusion plasmas," *Phys. Plasmas* **23**, 040702 (2016).
- ³⁰O. E. Garcia and A. Theodorsen, "Auto-correlation function and frequency spectrum due to a super-position of uncorrelated exponential pulses," *Phys. Plasmas* **24**, 032309 (2017).
- ³¹A. Theodorsen, O. E. Garcia, and M. Rypdal, "Statistical properties of a filtered Poisson process with additive random noise: Distributions, correlations and moment estimation," *Phys. Scr.* **92**, 054002 (2017).
- ³²A. Theodorsen and O. E. Garcia, "Level crossings and excess times due to a superposition of uncorrelated exponential pulses," *Phys. Rev. E* **97**, 012110 (2018).
- ³³A. Theodorsen and O. E. Garcia, "Probability distribution functions for intermittent scrape-off layer plasma fluctuations," *Plasma Phys. Controlled Fusion* **60**, 034006 (2018).
- ³⁴S. Ahmed, O. E. Garcia, and A. Theodorsen, "Reconstruction of intermittent time series as a superposition of pulses," *Phys. Rev. E* **107**, 054222 (2023).
- ³⁵O. E. Garcia, R. Kube, A. Theodorsen, and H. L. Pécseli, "Stochastic modelling of intermittent fluctuations in the scrape-off layer: Correlations, distributions, level crossings, and moment estimation," *Phys. Plasmas* **23**, 052308 (2016).
- ³⁶F. Militello and J. T. Omotani, "Scrape off layer profiles interpreted with filament dynamics," *Nucl. Fusion* **56**, 104004 (2016).
- ³⁷F. Militello and J. T. Omotani, "On the relation between non-exponential scrape off layer profiles and the dynamics of filaments," *Plasma Phys. Controlled Fusion* **58**, 125004 (2016).
- ³⁸N. R. Walkden, A. Wynn, F. Militello, B. Lipschultz, G. Matthews, C. Guillemaut, J. Harrison, D. Moulton, and JET Contributors, "Interpretation of scrape-off layer profile evolution and first-wall ion flux statistics on JET using a stochastic framework based on filamentary motion," *Plasma Phys. Controlled Fusion* **59**, 085009 (2017).
- ³⁹F. Militello, T. Farley, K. Mukhi, N. Walkden, and J. T. Omotani, "A two-dimensional statistical framework connecting thermodynamic profiles with filaments in the scrape off layer and application to experiments," *Phys. Plasmas* **25**, 056112 (2018).
- ⁴⁰J. M. Losada, A. Theodorsen, and O. E. Garcia, "Stochastic modelling of blob-like plasma filaments in the scrape-off layer: Theoretical foundation," *Phys. Plasmas* **30**, 042518 (2023).
- ⁴¹O. E. Garcia, N. H. Bian, V. Naulin, A. H. Nielsen, and J. J. Rasmussen, "Mechanism and scaling for convection of isolated structures in nonuniformly magnetized plasmas," *Phys. Plasmas* **12**, 090701 (2005).
- ⁴²J. Madsen, O. E. Garcia, J. Staerk Larsen, V. Naulin, A. H. Nielsen, and J. J. Rasmussen, "The influence of finite Larmor radius effects on the radial interchange motions of plasma filaments," *Phys. Plasmas* **18**, 112504 (2011).
- ⁴³R. Kube and O. E. Garcia, "Effect of dynamical friction on interchange motion of plasma filaments," *Phys. Plasmas* **19**, 042305 (2012).
- ⁴⁴M. Wiesenberger, J. Madsen, and A. Kendl, "Radial convection of finite ion temperature, high amplitude plasma blobs," *Phys. Plasmas* **21**, 092301 (2014).
- ⁴⁵J. Olsen, J. Madsen, A. H. Nielsen, J. J. Rasmussen, and V. Naulin, "Temperature dynamics and velocity scaling laws for interchange driven, warm ion plasma filaments," *Plasma Phys. Controlled Fusion* **58**, 044011 (2016).
- ⁴⁶H. L. Pécseli, D. S. Sortland, and O. E. Garcia, "A solvable blob-model for magnetized plasmas," *Plasma Phys. Controlled Fusion* **58**, 104002 (2016).
- ⁴⁷M. Held, M. Wiesenberger, J. Madsen, and A. Kendl, "The influence of temperature dynamics and dynamic finite ion Larmor radius effects on seeded high amplitude plasma blobs," *Nucl. Fusion* **56**, 126005 (2016).
- ⁴⁸M. Wiesenberger, M. Held, R. Kube, and O. E. Garcia, "Unified transport scaling laws for plasma blobs and depletions," *Phys. Plasmas* **24**, 064502 (2017).
- ⁴⁹M. Held and M. Wiesenberger, "Beyond the Oberbeck–Boussinesq and long wavelength approximation," *Nucl. Fusion* **63**, 026008 (2023).
- ⁵⁰O. E. Garcia, N. H. Bian, and W. Fundamenski, "Radial interchange motions of plasma filaments," *Phys. Plasmas* **13**, 082309 (2006).
- ⁵¹R. Kube and O. E. Garcia, "Velocity scaling for filament motion in scrape-off layer plasmas," *Phys. Plasmas* **18**, 102314 (2011).
- ⁵²P. Manz, D. Carralero, G. Birkenmeier, H. W. Müller, S. H. Müller, G. Fuchert, B. D. Scott, and U. Stroth, "Filament velocity scaling laws for warm ions," *Phys. Plasmas* **20**, 102307 (2013).
- ⁵³J. T. Omotani, F. Militello, L. Easy, and N. R. Walkden, "The effects of shape and amplitude on the velocity of scrape-off layer filaments," *Plasma Phys. Controlled Fusion* **58**, 014030 (2015).
- ⁵⁴N. R. Walkden, L. Easy, F. Militello, and J. T. Omotani, "Dynamics of 3D isolated thermal filaments," *Plasma Phys. Controlled Fusion* **58**, 115010 (2016).
- ⁵⁵S. I. Krasheninnikov, "On scrape off layer plasma transport," *Phys. Lett. A* **283**, 368–370 (2001).
- ⁵⁶D. A. D'Ippolito, J. R. Myra, and S. I. Krasheninnikov, "Cross-field blob transport in tokamak scrape-off-layer plasmas," *Phys. Plasmas* **9**, 222 (2002).
- ⁵⁷J. R. Myra, D. A. Russell, and D. A. D'Ippolito, "Collisionality and magnetic geometry effects on tokamak edge turbulent transport. I. A two-region model with application to blobs," *Phys. Plasmas* **13**, 112502 (2006).
- ⁵⁸L. Easy, F. Militello, J. Omotani, B. Dudson, E. Havlickova, P. Tamain, V. Naulin, and A. H. Nielsen, "Three dimensional simulations of plasma filaments in the scrape off layer: A comparison with models of reduced dimensionality," *Phys. Plasmas* **21**, 122515 (2014).
- ⁵⁹F. D. Halpern, A. Cardellini, P. Ricci, S. Jolliet, J. Loizu, and A. Masetto, "Three-dimensional simulations of blob dynamics in a simple magnetized torus," *Phys. Plasmas* **21**, 022305 (2014).
- ⁶⁰L. Easy, F. Militello, J. Omotani, N. R. Walkden, and B. Dudson, "Investigation of the effect of resistivity on scrape off layer filaments using three-dimensional simulations," *Phys. Plasmas* **23**, 012512 (2016).
- ⁶¹A. Theodorsen, O. E. Garcia, J. Horacek, R. Kube, and R. A. Pitts, "Scrape-off layer turbulence in TCV: Evidence in support of stochastic modelling," *Plasma Phys. Controlled Fusion* **58**, 044006 (2016).
- ⁶²O. E. Garcia, I. Cziegler, R. Kube, B. LaBombard, and J. L. Terry, "Burst statistics in Alcator C-Mod SOL turbulence," *J. Nucl. Mater.* **438**, S180–S183 (2013).
- ⁶³O. E. Garcia, S. M. Fritznier, R. Kube, I. Cziegler, B. LaBombard, and J. L. Terry, "Intermittent fluctuations in the Alcator C-Mod scrape-off layer," *Phys. Plasmas* **20**, 055901 (2013).
- ⁶⁴O. E. Garcia, J. Horacek, and R. A. Pitts, "Intermittent fluctuations in the TCV scrape-off layer," *Nucl. Fusion* **55**, 062002 (2015).
- ⁶⁵R. Kube, A. Theodorsen, O. E. Garcia, B. LaBombard, and J. L. Terry, "Fluctuation statistics in the scrape-off layer of Alcator C-Mod," *Plasma Phys. Controlled Fusion* **58**, 054001 (2016).
- ⁶⁶O. E. Garcia, R. Kube, A. Theodorsen, J. G. Bak, S. H. Hong, H. S. Kim, KSTAR Project Team, and R. A. Pitts, "SOL width and intermittent fluctuations in KSTAR," *Nucl. Mater. Energy* **12**, 36–43 (2017).
- ⁶⁷O. E. Garcia, R. Kube, A. Theodorsen, B. LaBombard, and J. L. Terry, "Intermittent fluctuations in the Alcator C-Mod scrape-off layer for ohmic and high confinement mode plasmas," *Phys. Plasmas* **25**, 056103 (2018).
- ⁶⁸R. Kube, O. E. Garcia, A. Theodorsen, A. Q. Kuang, B. LaBombard, J. L. Terry, and D. Brunner, "Statistical properties of the plasma fluctuations and turbulent cross-field fluxes in the outboard mid-plane scrape-off layer of Alcator C-Mod," *Nucl. Mater. Energy* **18**, 193–200 (2019).
- ⁶⁹A. Q. Kuang, B. LaBombard, D. Brunner, O. E. Garcia, R. Kube, and A. Theodorsen, "Plasma fluctuations in the scrape-off layer and at the divertor target in Alcator C-Mod and their relationship to divertor collisionality and density shoulder formation," *Nucl. Mater. Energy* **19**, 295–299 (2019).
- ⁷⁰R. Kube, A. Theodorsen, O. E. Garcia, D. Brunner, B. Labombard, and J. L. Terry, "Comparison between mirror Langmuir probe and gas-puff imaging measurements of intermittent fluctuations in the Alcator C-Mod scrape-off layer," *J. Plasma Phys.* **86**, 905860519 (2020).
- ⁷¹A. Bencze, M. Berta, A. Buzás, P. Hacek, J. Krbec, and M. Sztyányi, "Characterization of edge and scrape-off layer fluctuations using the fast Li-

- BES system on COMPASS,” *Plasma Phys. Controlled Fusion* **61**, 085014 (2019).
- ⁷²S. J. Zweben, M. Lampert, and J. R. Myra, “Temporal structure of blobs in NSTX,” *Phys. Plasmas* **29**, 072504 (2022).
- ⁷³S. Ahmed, O. E. Garcia, A. Q. Kuang, B. LaBombard, J. L. Terry, and A. Theodorsen, “Strongly intermittent far scrape-off layer fluctuations in Alcator C-Mod plasmas close to the empirical discharge density limit,” *Plasma Phys. Controlled Fusion* **65**, 105008 (2023).
- ⁷⁴O. E. Garcia, N. H. Bian, V. Naulin, A. H. Nielsen, and J. J. Rasmussen, “Two-dimensional convection and interchange motions in fluids and magnetized plasmas,” *Phys. Scr.* **T122**, 104–124 (2006).
- ⁷⁵C. Theiler, I. Furno, A. Fasoli, P. Ricci, B. Labit, and D. Iraj, “Blob motion and control in simple magnetized plasmas,” *Phys. Plasmas* **18**, 055901 (2011).
- ⁷⁶R. Kube, O. E. Garcia, B. LaBombard, J. L. Terry, and S. J. Zweben, “Blob sizes and velocities in the Alcator C-Mod scrape-off layer,” *J. Nucl. Mater.* **438**, S505–S508 (2013).
- ⁷⁷G. Fuchert, G. Birkenmeier, B. Nold, M. Ramisch, and U. Stroth, “The influence of plasma edge dynamics on blob properties in the stellarator TJ-K,” *Plasma Phys. Controlled Fusion* **55**, 125002 (2013).
- ⁷⁸G. Fuchert, G. Birkenmeier, D. Carralero, T. Lunt, P. Manz, H. W. Müller, B. Nold, M. Ramisch, V. Rohde, and U. Stroth, “Blob properties in L- and H-mode from gas-puff imaging in ASDEX upgrade,” *Plasma Phys. Controlled Fusion* **56**, 125001 (2014).
- ⁷⁹S. J. Zweben, J. R. Myra, W. M. Davis, D. A. D’Ippolito, T. K. Gray, S. M. Kaye, B. P. Leblanc, R. J. Maqueda, D. A. Russell, and D. P. Stotler, “Blob structure and motion in the edge and SOL of NSTX,” *Plasma Phys. Controlled Fusion* **58**, 044007 (2016).
- ⁸⁰D. Carralero, M. Siccinio, M. Komm, S. A. Artene, F. A. D’Isa, J. Adamek, L. Aho-Mantila, G. Birkenmeier, M. Brix, G. Fuchert, M. Groth, T. Lunt, P. Manz, J. Madsen, S. Marsen, H. W. Müller, U. Stroth, H. J. Sun, N. Vianello, M. Wischmeier, and E. Wolfrum, “Recent progress towards a quantitative description of filamentary SOL transport,” *Nucl. Fusion* **57**, 056044 (2017).
- ⁸¹G. Decristoforo, F. Militello, T. Nicholas, J. Omotani, C. Marsden, N. Walkden, and O. E. Garcia, “Blob interactions in 2D scrape-off layer simulations,” *Phys. Plasmas* **27**, 122301 (2020).
- ⁸²W. Han, N. Offeddu, T. Golfopoulos, C. Theiler, J. L. Terry, C. Wüthrich, D. Galassi, C. Colandrea, E. S. Marmor, and TCV Team, “Estimating cross-field particle transport at the outer midplane of TCV by tracking filaments with machine learning,” *Nucl. Fusion* **63**, 076025 (2023).
- ⁸³M. A. Korzeniewska, A. Theodorsen, M. Rypdal, and O. E. Garcia, “Apparent universality of $1/f$ spectra as an artifact of finite-size effects,” *Phys. Rev. Res.* **5**, L022066 (2023).
- ⁸⁴B. LaBombard, M. V. Umansky, R. L. Boivin, J. A. Goetz, J. Hughes, B. Lipschultz, D. Mossessian, C. S. Pitcher, and J. L. Terry, “Cross-field plasma transport and main-chamber recycling in diverted plasmas on Alcator C-Mod,” *Nucl. Fusion* **40**, 2041–2060 (2000).
- ⁸⁵B. Lipschultz, B. LaBombard, C. S. Pitcher, and R. Boivin, “Investigation of the origin of neutrals in the main chamber of Alcator C-Mod,” *Plasma Phys. Controlled Fusion* **44**, 733–748 (2002).
- ⁸⁶J. A. Boedo, D. L. Rudakov, R. J. Colchin, R. A. Moyer, S. Krashennikov, D. G. Whyte, G. R. McKee, G. Porter, M. J. Schaffer, P. C. Stangeby, W. P. West, S. L. Allen, and A. W. Leonard, “Intermittent convection in the boundary of DIII-D,” *J. Nucl. Mater.* **313–316**, 813–819 (2003).
- ⁸⁷D. G. Whyte, B. L. Lipschultz, P. C. Stangeby, J. Boedo, D. L. Rudakov, J. G. Watkins, and W. P. West, “The magnitude of plasma flux to the main-wall in the DIII-D tokamak,” *Plasma Phys. Controlled Fusion* **47**, 1579–1607 (2005).
- ⁸⁸B. LaBombard, J. W. Hughes, D. Mossessian, M. Greenwald, B. Lipschultz, and J. L. Terry, “Evidence for electromagnetic fluid drift turbulence controlling the edge plasma state in the Alcator C-Mod tokamak,” *Nucl. Fusion* **45**, 1658–1675 (2005).
- ⁸⁹B. Lipschultz, D. Whyte, and B. LaBombard, “Comparison of particle transport in the scrape-off layer plasmas of Alcator C-Mod and DIII-D,” *Plasma Phys. Controlled Fusion* **47**, 1559–1578 (2005).
- ⁹⁰D. L. Rudakov, J. A. Boedo, R. A. Moyer, P. C. Stangeby, J. G. Watkins, D. G. Whyte, L. Zeng, N. H. Brooks, R. P. Doerner, T. E. Evans, M. E. Fenstermacher, M. Groth, E. M. Hollmann, S. I. Krashennikov, C. J. Lasnier, A. W. Leonard, M. A. Mahdavi, G. R. McKee, A. G. McLean, A. Y. Pigarov, W. R. Wampler, G. Wang, W. P. West, and C. P. Wong, “Far SOL transport and main wall plasma interaction in DIII-D,” *Nucl. Fusion* **45**, 1589–1599 (2005).
- ⁹¹J. Horacek, R. A. Pitts, and J. P. Graves, “Overview of edge electrostatic turbulence experiments on TCV,” *Czech. J. Phys.* **55**, 271–283 (2005).
- ⁹²O. E. Garcia, J. Horacek, R. A. Pitts, A. H. Nielsen, W. Fundamenski, J. P. Graves, V. Naulin, and J. J. Rasmussen, “Interchange turbulence in the TCV scrape-off layer,” *Plasma Phys. Controlled Fusion* **48**, L1–L10 (2006).
- ⁹³G. Y. Antar, M. Tsalas, E. Wolfrum, and V. Rohde, “Turbulence during H- and L-mode plasmas in the scrape-off layer of the ASDEX Upgrade tokamak,” *Plasma Phys. Controlled Fusion* **50**, 095012 (2008).
- ⁹⁴D. Carralero, H. W. Müller, M. Groth, M. Komm, J. Adamek, G. Birkenmeier, M. Brix, F. Janky, P. Hecce, S. Marsen, F. Reimold, C. Silva, U. Stroth, M. Wischmeier, and E. Wolfrum, “Implications of high density operation on SOL transport: A multimachine investigation,” *J. Nucl. Mater.* **463**, 123–127 (2015).
- ⁹⁵F. Militello, L. Garzotti, J. Harrison, J. T. Omotani, R. Scannell, S. Allan, A. Kirk, I. Lupelli, and A. J. Thornton, “Characterisation of the L-mode scrape off layer in MAST: Decay lengths,” *Nucl. Fusion* **56**, 016006 (2016).
- ⁹⁶N. Vianello, C. Tsui, C. Theiler, S. Allan, J. Boedo, B. Labit, H. Reimerdes, K. Verhaegh, W. A. J. Vijvers, N. Walkden, S. Costea, J. Kovacic, C. Ionita, V. Naulin, A. H. Nielsen, J. J. Rasmussen, B. Schneider, R. Schrittwieser, M. Spolaore, D. Carralero, J. Madsen, B. Lipschultz, F. Militello, TCV Team, and EUROfusion MST1 Team, “Modification of SOL profiles and fluctuations with line-average density and divertor flux expansion in TCV,” *Nucl. Fusion* **57**, 116014 (2017).
- ⁹⁷A. Wynn, B. Lipschultz, I. Cziegler, J. Harrison, A. Jaervinen, G. F. Matthews, J. Schmitz, B. Tal, M. Brix, C. Guillemaut, D. Frigione, A. Huber, E. Joffrin, U. Kruzei, F. Militello, A. Nielsen, N. R. Walkden, and S. Wiesen, “Investigation into the formation of the scrape-off layer density shoulder in JET ITER-like wall L-mode and H-mode plasmas,” *Nucl. Fusion* **58**, 056001 (2018).
- ⁹⁸N. Vianello, D. Carralero, C. K. Tsui, V. Naulin, M. Agostini, I. Cziegler, B. Labit, C. Theiler, E. Wolfrum, D. Aguiam, S. Allan, M. Bernert, J. Boedo, S. Costea, H. D. Oliveira, O. Fevrier, J. Galdon-Quiroga, G. Grenfell, A. Hakola, C. Ionita, H. Isliker, A. Karpushov, J. Kovacic, B. Lipschultz, R. Maurizio, K. McClements, F. Militello, A. H. Nielsen, J. Olsen, J. J. Rasmussen, T. Ravensbergen, H. Reimerdes, B. Schneider, R. Schrittwieser, E. Selinunin, M. Spolaore, K. Verhaegh, J. Vicente, N. Walkden, W. Zhang, ASDEX Upgrade Team, TCV Team, and EUROfusion MST1 Team, “Scrape-off layer transport and filament characteristics in high-density tokamak regimes,” *Nucl. Fusion* **60**, 016001 (2020).
- ⁹⁹A. Stagni, N. Vianello, C. K. Tsui, C. Colandrea, S. Gorno, M. Bernert, J. A. Boedo, D. Brida, G. Falchetto, A. Hakola, G. Harrer, H. Reimerdes, C. Theiler, E. Tsitrone, N. Walkden, the TCV Team, and the EUROfusion MST1 Team, “Dependence of scrape-off layer profiles and turbulence on gas fuelling in high density H-mode regimes in TCV,” *Nucl. Fusion* **62**, 096031 (2022).
- ¹⁰⁰G. Decristoforo, A. Theodorsen, J. Omotani, T. Nicholas, and O. E. Garcia, “Numerical turbulence simulations of intermittent fluctuations in the scrape-off layer of magnetized plasmas,” *Phys. Plasmas* **28**, 072301 (2021).